THE SURFACE BRIGHTNESS PROFILES OF ELLIPTICAL AND SUPERGIANT GALAXIES

Darlene A. English

A thesis submitted as
partial requirement
for the degree of
Master of Science
from
Saint Mary's University

Department of Astronomy
Saint Mary's University
1979

TABLE OF CONTENTS

ACKNOWLEDGEMENTS

I would like to thank the many people who offered comments, suggestions, and encouragement during the work on this thesis. A very special thank you goes to my thesis supervisor, Dr. Gary A. Welch, for suggesting this topic, and for allowing me the use of his data and the reduction program PROFIL. His patient guidance made the completion of this thesis possible.

ABSTRACT

The surface brightness profiles of a sample of supergiant and elliptical galaxies were studied. The original data were gathered by Dr. G.A. Welch, who also wrote the program (PROFIL) for the data reduction.

This study was undertaken at the suggestion of Dr. Welch, to investigate the shape of the brightness profiles of several supergiant galaxies, and to determine if they fit the relation recently suggested for cD galaxies by Bahcall (1977). Data from a number of elliptical galaxies was also processed using the same methods as a check on the reduction procedures. The cD galaxies were calibrated directly using photoelectric photometry, while the profiles of the elliptical galaxies were put on an absolute scale utilizing a photographic transfer method.

Based on comparisons with published profiles for several of the galaxies, the resulting brightness profiles were found not to contain any significant errors due to calibration or reduction procedures. The elliptical galaxies (with one exception) all fit the de Vaucouleurs (1953) relation for ellipticals, as expected. The exception, a galaxy identified as A-29/52 AC, appears to have a brightness profile which shows an extended halo, and also fits very well the relation suggested by Bahcall

for the profiles of cD galaxies. AC does not appear to be located in a cluster.

Three of the four cD galaxies studied show good agreement with the Bahcall relation. The fourth, the cD galaxy in Abell 401, displays a much shallower decline in brightness than the other program cD galaxies, and with respect to the Bahcall relation. It is thus concluded that all supergiant galaxies do not fit the Bahcall relation, and that there are other objects, not classified as cD galaxies, whose light distributions do seem to fit the Bahcall relation.

This finding holds important implications for the investigation of the dynamical history of supergiant galaxies, as the evolutionary paths of galaxies whose brightness profiles obey a particular empirical relation may be different from those galaxies whose profiles do not.

1.) INTRODUCTION

1.1 Historical Review

The supergiant galaxies, originally classified by Matthews, Morgan, and Schmidt (1964), were considered to have the following characteristics:

(1) all were located in clusters, of which they were the brightest and largest members;

(2) all were centrally located in the clusters;

(3) the objects were never highly elliptical in shape;

(4) the objects had a bright, elliptical-like nucleus, surrounded by an extended halo.

These galaxies were similar in appearance to the D galaxies of Morgan's (1958) classification, but due to their large size and luminosity, the prefix "c" was assigned, giving cD by analogy to the notation used for supergiant stars in the old stellar classification system.

Matthews et al. found that approximately half of all known extragalactic radio sources could be identified with bright cD galaxies. Studies of Abell clusters (eg. Morgan and Lesh 1965; Bautz and Morgan 1970; Leir and van den Bergh 1977) have found that $\sim$20 % of rich clusters of galaxies contain a central, dominant cD galaxy. However, poor clusters containing cD galaxies have been detected (Morgan, Kayser,

and White 1975; Albert, White, and Morgan 1977). It is not yet known if any fundamental differences exist between the cD galaxies in rich and poor clusters.

Frequently, the supergiant galaxy halo envelops multiple nuclei (eg. NGC 6166), and mass estimates are available for several such galaxies from the virial theorem (Jenner 1974; Minkowski 1961; Page 1961). These estimates are typically on the order of 10^{13} $M_{\odot}$.

An area in which the understanding of supergiant galaxies is important is the study of cluster dynamics and evolution. Under active investigation are the questions of how cD galaxies are formed, why they form in some clusters and not in others, and their possible contribution to the evolution of a cluster.

Current ideas on the formation and evolution of cD galaxies are based on their growth from other material in the cluster. Alternatively, Geller (1974) has suggested that supergiant galaxies are merely the bright end of the luminosity function. Ostriker and Tremaine (1975), Ostriker and Hausman (1977), Hausman and Ostriker (1978), and others have discussed the results of close encounters between galaxies at the centre of a cluster. These would cause the smaller galaxy to be captured (cannibalized) by the larger by means of dynamical friction, resulting in the growth of a very large galaxy at the centre of the cluster potential

well. Multiple nuclei within the cD envelope are explained as stripped nuclei of ordinary galaxies which have been captured by the cD galaxy.

This theory predicts that the first-ranked galaxies of rich, compact clusters should have much larger total luminosities than those of poorer, less dense clusters. Studies by Sandage (1976) have shown that there is a small correlation of brightest-cluster galaxy luminosity with cluster richness, while Oemler (1976) has found that there is a strong tendency for the total luminosity of the extended halos of cD galaxies to be a function of cluster richness.

Gallagher and Ostriker (1972) and Richstone (1976) have suggested that tidal interactions between cluster galaxies could strip off their outer envelopes. This material would be released into intergalactic space to eventually be drawn towards the centre of the cluster's potential well, where it would be added to material already present. Strom and Strom (1978a, b, d) have found that elliptical galaxies located in the higher density core regions of the spiral-poor clusters of Perseus and Coma, and the cD cluster Abell 2199 tend to have smaller effective radii, compared to elliptical galaxies in the outer regions of these clusters. This observation could be interpreted as tidal stripping of the halos of the ellipticals due to interactions.

From this debris hypothesis of cD formation follow several predictions:

(1) The velocity dispersion of the stars in the cD galaxy envelope should reflect that of the galaxies in the cluster. That is, it should be much larger than the dispersion within the outer regions of a normal galaxy. Faber, Burstein, and Dressler (1977) have shown however, that the halo of the cD galaxy in Abell 401 is not entirely composed of stars with velocity dispersions typical of cluster galaxies. They suggest the possibility that a high-velocity dispersion cD halo may form about an existing low-velocity dispersion elliptical galaxy. Their observations are also consistent, however, with the hypothesis that cD galaxies are bright, but normal ellipticals at the bright end of the luminosity function.

(2) The cluster profile should be centred on the bottom of the cluster potential well. In addition, Oemler (1973) has found that the envelope surface brightness profile of the cD galaxy in Abell 2670 matches the cluster luminosity profile quite closely. This is both consistent with, and expected of, the debris hypothesis and the galaxy cannibalism theory.

(3) Since the material which formed the halo of the cD galaxy was originally stripped from the outer regions of other galaxies, the cD halo should be lacking in colour gradients. The mass-to-light ratio should also be

that of the outer regions of the galaxies from which it was formed. Strom and Strom (1976, 1978b) have found evidence that the envelopes of elliptical galaxies are in general, bluer and more metal-poor than the central regions. Measurements of absorption line strengths in the halo of the cD galaxy in Abell 401 by Faber et al. have shown that the halo population at 43 kpc is close to the average of the stars in the solar neighbourhood.

(4) There should be a decrease in luminosity in the galaxies of the cluster as the cD galaxy grows at their expense. Thus, as Sandage and Hardy (1973) noted, the second- and third-ranked cluster galaxies are fainter, with respect to the brightest galaxy, than would normally be expected. This phenomenon is also predicted for the cannibalism theory, since Oemler (1974) has found evidence that mass-segregation in cD clusters may be common.

The study of supergiant galaxy brightness profiles is therefore important to our understanding of their formation. Some fundamental questions yet to be satisfactorially answered are: Do all objects classified as cD galaxies have the same light distribution? Are there other objects whose surface brightness profiles are the same shape as the "classical" cD galaxies (ie. satisfying the criteria used by Matthews et al.)?

Recent work by Oemler (1973, 1974, 1976) and Carter

(1977) has shown the great extent of these galaxies. Their radii range from 100 kpc for NGC 4073, to almost 2 Mpc for the cD galaxy in Abell 1413. These studies have also shown that there is a distinct difference in the shapes of the surface brightness profiles of normal elliptical and supergiant galaxies. Most elliptical galaxy profiles can be fit to de Vaucouleurs' (1953) law, one of King's (1962) models, or to Oemler's (1976) reduced Hubble law. The cD galaxy, however, cannot be accomodated by these relations. The light distribution in the inner parts of the cD galaxy is similar to that of a normal giant elliptical, but the above laws fail to match the brightness of its enormous extended halo. De Vaucouleurs (1974) has noted that the luminosity of the outer regions of the cD galaxy seems to decline exponentially, while Bahcall (1977) has suggested a general relation which (roughly) fits cD profiles (excluding the central portions $R < 5$ kpc).

1.2 Aim of this Thesis

The present investigation aims to expand our knowledge of the differences between normal elliptical and supergiant galaxy brightness profiles, and to examine whether Bahcall's law will indeed fit the halo profiles of all supergiants. To this end, four cD galaxies have been chosen, all from relatively rich Abell clusters. Little or no work had been

done on their light distributions, except for NGC 6166 in Abell 2199 (see Oemler 1976; Carter 1977). Photoelectric photometry was available from the literature for most of the galaxies.

Nine elliptical galaxies were also chosen to compare with cD profiles, and to test the reduction procedures. This number included the giant elliptical NGC 4881 for which previous profiles (Strom and Strom 1978a; Oemler 1976) were available for direct comparison of results. Three elliptical galaxies were chosen from the plate in the field of each cD galaxy, except for the plates containing Abell 2029 and 2052, from which only two ellipticals were used.

The eight ellipticals in this study were chosen using the following criteria:

(1) they were all normal-appearing elliptical galaxies with low eccentricity; and

(2) all were approximately the same apparent size and brightness as the cD galaxy on that plate.

2.) DATA SOURCES

2.1 Observations

Plate material for this study was obtained by Dr. G.A. Welch during observing sessions in May 1970, and June and September of 1971 on the 1.2m (48 inch) Palomar Schmidt Telescope. Emulsion-filter combinations (see Appendix A) were used to obtain plates in three bandpasses. 103a-E emulsion with a Chance OR-1 filter was used for the R bandpass (centred at approximately 6600 Å), the V bandpass (5400 Å) was obtained using 103a-D emulsion with a Kodak Wratten 12 filter, while IIIa-J with Wratten 4 gave the J bandpass (5100 Å). In the case of plate PS 6863, IIIa-J and Wratten 2c were used to produce a slightly different bandpass (4700 Å). Hereafter, the emulsion-filter combinations will be referred to by the name of their bandpass (ie. R, V, and J).

All IIIa-J plates were baked in air at 65 C for six hours before use. The developing procedure was the same for all three runs. Plates were developed in MWP-2 for eight minutes (except the IIIa-J plates, which were developed for eleven minutes). All plates were calibrated using the spot sensitometer in the 1.2m darkroom and a relative intensity calibration provided by Dr. J. Kormendy. The 103a-D plates were exposed for 10 minutes through a

yellow filter, while a combination of blue and yellow filters with a 60 minute exposure was used to produce the spots on the IIIa-J plates.

The photoelectric photometry, also by Dr. Welch, was done on three separate occasions. In February and March of 1970, the #1 offset photometer with a 1P21 photomultiplier tube and DC electronics was used on the #2 0.9m (36 inch) telescope at Kitt Peak National Observatory. The third run was during October of 1971, on the KPNO 1.3m (50 inch). The same photometer and PMT were used as for the previous observations, but with pulse counting electronics. On all occasions diaphragm #8 was used, and a Corning #3304 filter used for the V bandpass.

Table I gives the 1950 coordinates and approximate classifications for all galaxies in this study, as well as an estimate of their apparent magnitude, and references.

2.2 Densitometry

Density tracings (a graph of relative image density versus position) were made of the program galaxies from the plates using the Joyce-Loebl microdensitometer at Michigan State University. The tracings were made along the major axis of a galaxy, passing through the nucleus. In all cases angular alignment was done by eye, choosing the nucleus as the point of maximum image density. For

TABLE I

Program Galaxies

GALAXY	COORDINATES (1950) α	δ	APPARENT V mag.	CLASSIFICATION	
A401 cD	$02^h56^m.7$	+13°27'	--	cD	
#1	02 49.2	+13 58	--	E1-S0	†
#2	02 51.7	+15 33.8	--	E1	†
#3	02 50.9	+13 35.0	--	E2	†
A2029 cD	15 08.2	+05 57	15.4	cD	
#5	15 08.5	+06 59	15.4	E0	†
AC	15 16.5	+04 42	15.0	S0	†
A2052 cD	15 14.3	+07 12	14.8	cD	
NGC 6166	16 26.9	+39 40	13.9	cD	
NGC 6146	16 23.5	+41 01	13.8	E2-3	
NGC 6160	16 26.0	+41 02	14.8	E2	
NGC 6173	16 28.1	+40 55	14.0	E3	
NGC 4881	12 57.5	+28 31	14.8	E1	

References:

-all apparent magnitudes and classifications:

Nilson (1973) Uppsala General Catalogue of Galaxies

except † :

Welch (this study).

the ellipticals classified as E0, where no major axis was evident, the tracing was aligned east-west. In cases where the central region of the image was very dark, this procedure was sometimes unable to locate the maximum density point with certainty, and this could result in the tracing missing the nucleus (see discussion in section 3.4). The scale of the tracing was adjusted so that the entire visible extent of the galaxy filled the graph paper.

In addition, tracings of the sky density near each galaxy were made at the same position angle. These tracings covered 50mm on the plate (equal to 56') and were centred on the program galaxy.

The density tracings were digitized using the digitization table of the Geology Department at Michigan State University. The instrument employed a cursor which was guided carefully by hand over the curve. At intervals of approximately 1mm in one coordinate, values of X and Y accurate to ±0.1mm were automatically punched on a computer card. The (X, Y) values so obtained related to an internal Cartesian system which, in general, differed from the (density, position) coordinates on the tracing paper by an unknown angle of rotation. To enable determination of this angle, and therefore to allow conversion of (X, Y) into (density, position), the coordinates of three reference grid points on the tracing paper were also measured. These

coordinates were again measured after digitizing the tracing as a check on possible movement of the paper during the process. When digitizing the sky tracings, the regions surrounding the galaxy and any obvious field objects were excluded.

Isodensity tracings (plots of equal image density in the region of a galaxy) were made by the isodensitracer at Michigan State University of all the program galaxies except the ellipticals A-401 #1, #2, and #3. However, only the isodents of the four cD galaxies and NGC 6173 could be used for calibration of the brightness profiles, due to the lack of available photometry for the other galaxies.

Characteristic curves for each plate were constructed by hand from the spot sensitometry. The typical curve was nearly linear in the region actually used. In particular, the IIIa-J plates were purposely exposed to put the faint outer regions of the galaxy images on the linear portion of the curve. After construction of the curve, 20 to 30 points, equally spaced in density, were chosen to be input for the program PROFIL to represent the density-relative intensity relation for that plate.

3.) THE PROGRAM PROFIL

3.1 Purpose of the Program

The computer program PROFIL was written by Dr. Welch and runs on the Dalhousie University Computer Centre's CDC 6400. It converts the relative density data from the plates to plots of relative intensity versus position within the galaxy, ie. a surface brightness profile. A copy of the program is available on request from the author or from Dr. Welch.

3.2 Reduction of Individual Density Tracings

The data from the density tracings and the characteristic curves are input in the form of punched cards. The density points are then converted to values relative to the clear plate density. Any point whose density is less than the first point on the characteristic curve is assigned a negative intensity value and is removed from subsequent processing. Each density point is then run through the characteristic curve using two-difference Gregory-Newton interpolation to assign appropriate relative intensities. Results of this interpolation agree with hand reductions to within the accuracy with which densities can be obtained from the tracings (±0.1mm on the tracing paper).

The program then performs a linear least squares fit

on data input from a low magnification density tracing of each galaxy to obtain the sky level. The slope of this line is printed out to allow identification of tracings where significant changes occur over the extent of the galaxy. Standard deviations of scatter about this line are also computed and printed out in the form of the intensity σ_{sky}. After the sky fog level at the location of the galaxy is assigned a relative intensity, it is subtracted from the galaxy intensities. These points, together with their corresponding radial positions in seconds of arc, are then divided into two sets, one for each semi-major axis of the galaxy.

3.3 Stacking of Data from Different Plates

The "stacking" of several tracings of the same galaxy was done for two reasons. Averaging tracings from long and short exposure plates allows a larger range of surface brightness to be covered. The stacking of several density tracings from plates of different exposures was done to increase the signal-to-noise ratio of the resulting profile, as the averaging process cancels out much of the random noise in the individual tracings. However, since only two exposures in one bandpass (the V) were available for stacking, a further increase in the signal-to-noise ratio was achieved by the averaging of exposures from different

bandpasses.

The data sets can then be treated in four different ways. The option NO AVERAGE specifies that the intensity profile of each semi-major axis is to be plotted separately. AVERAGE1ST produces an average of the intensity profile of the first semi-major axis on a specified number (NPLATE) of plates. AVERAGE2ND averages and plots profiles of the second semi-major axis. AVERAGEALL will average both semi-axes of each tracing before averaging in the next density tracing.

The final output of PROFIL includes:

IDENT galaxy identification

IPLATE plate number

IEXP plate exposure and bandpass

L1, L2 projected dimensions of microdensitometer slit

In addition, the program prints out the digital data taken from the density tracing (IOBJ), and sky tracing (ISKY), and the points defining the characteristic curve (CURVE). NO AVERAGE produces a graph of log I versus log R (I is the relative intensity, R is the radial distance in arcseconds) for each semi-major axis. As each density profile is reduced, AVERAGE1ST and AVERAGE2ND produce two graphs of log I versus log R. The first graph displays the average of all previous profiles and shows the current profile shifted in log I to give the best fit with the average.

The second graph shows the new average. AVERAGEALL also prints out two graphs for each input tracing. First, the two semi-axes are shown folded onto a single log I versus log R plot. An average profile is then computed. The second graph displays this profile combined with the cumulative average of the previous tracings. Thus, in stacking runs, the final graph represents the average of one or both semi-major axes of all input tracings.

During the averaging process, the program chooses a segment of each profile to serve as a matching region. The inner boundary of this region is defined as the first point at which log I is less than 2.97 (on a scale on which the point of maximum intensity is log I = 3.00), or R is greater than twice the angular slit width of the microdensitometer. The outer boundary is defined by the first point at which the relative intensity exceeds that of the sky by $20\sigma_{sky}$. A least squares criterion is then applied to the matching regions in order to determine the amount by which the current profile must be shifted in log I. If the intersection of the matching regions of the cumulative average and the current profile contains fewer than 25 points, the profile is dropped from the stacking run.

Special adjustments of these criteria had to be made in order to stack the tracings for the cD galaxy in

Abell 401. It was discovered that due to the shallow slope of the brightness profile and the relative brightness of the sky level, a matching region of acceptable length could not be produced using the criteria stated above. In order to circumvent this problem, the inner boundary was moved inward to one slit width from the centre, and the outer boundary extended to an intensity of $12.5\sigma_{sky}$. The same increases in boundary criteria had to be used to stack tracings from the elliptical galaxies A-401 #1, #2, and #3 which were located on the same plates as Abell 401. The cD galaxy in Abell 2029 also required the same new criteria ($12.5\sigma_{sky}$ and one slit width), while the elliptical galaxy A-29/52 #5 needed $12.5\sigma_{sky}$ with two slit widths to stack all tracings.

The brightest point in the first tracing to be averaged was arbitrarily assigned log I = 3.00. When all subsequent profiles were moved vertically in log I so that their matching regions fit those previously averaged, the intensity scale was shifted, if necessary, so that the brightest point remained at log I = 3.00. Whenever the shifting of the scale was required, the amount of movement was recorded.

3.4 Sources of Error

Careful examination of the stacked profiles of each galaxy sometimes revealed anomolies in the profiles from individual plates. Most commonly, it was found that both axes of the anomolous profile were noticeabley fainter near the nucleus than the average of the other profiles. It was assumed that the original density tracing had missed the nucleus (see section 2.2), and the tracing was therefore omitted. As this problem occurred only with the IIIa-J plates, it was probably due to the difficultly in locating the true density maximum in the heavily exposed central region of the galaxy.

In the case of the cD galaxy in Abell 2029, the tracing from plate PS 6863 produced a profile which, north of the nucleus, was brighter in the inner regions than the average of the other four profiles, and fainter than the average to the south of the nucleus. It was also observed that on this profile the position of "bumps" corresponding to field objects were systematically different than on the average profile. The conclusion was that the wrong position had been assigned to the centre of the galaxy on the original density record, thus shifting all of the radial coordinates to the north.

The problem was solved by examining the density tracing for this plate and recomputing the coordinates for the

galaxy centre, using the known grid coordinates. With the substitution of the new value, the anomoly was eliminated.

Another problem encountered was that of inaccurate determination of the sky level to be subtracted. It was discovered through examination of the sky density tracings, that large-scale variations in the sky fog in the immediate vicinity of the galaxy made several of the calculated values for the sky levels inappropriate for one or both axes of the galaxy. In these cases (only in tracings from the IIIa-J plates), the appropriate sky level was determined by fitting a straight line by eye to each axis directly on the sky and/or galaxy tracing. The same procedure was used when the program found relatively large density gradients in the sky fog. These values were then assigned within the program PROFIL to replace the inappropriate values (see Appendix C). Inhomogeneities in plate fog on the IIIa-J plates were probably the result of baking in air.

An incorrect sky level can seriously alter the shape of the resulting brightness profile at faint light levels. If the sky level used is too low, then a profile whose outer regions are too bright will be produced. Faint outer regions with an abnormally sharp cut-off would result if the sky level were chosen too high. As an example, a change in the sky level of 2mm in relative density of the SW axis of the cD galaxy in Abell 401 produced a change of

approximately 0.5 magnitudes per square arcsecond in surface brightness $\mu(r)$.

4.) CALIBRATION OF SURFACE BRIGHTNESS PROFILES

4.1 Calibration from Photoelectric Photometry

Calibration of the computer-generated relative intensity profiles in terms of standard surface brightness in magnitudes per square arcsecond was accomplished by two different methods. The first method involved direct calibration using photoelectric photometry, and was used for all of the cD galaxies. Sources of the photometry are Welch (present study) for Abell 401 and Abell 2029, and Sandage (1972) for NGC 6166 and Abell 2052. In addition, the direct calibration of the elliptical galaxy NGC 6173 was possible using the photometry of Peterson (1970).

Using tracing paper over the isodensity tracings of the above named galaxies, smoothed copies of their isophotes were obtained. A photometric aperture of an appropriate size was then drawn, centred at the nucleus. This centre position was determined from the average of the centre points of all of the isophotes, as measured along the major axis. For NGC 6166 and 6173, the interiors were too dense to be registered on the isodensity tracings and additional isophotes were constructed by eye about each nucleus, having approximately the same shape as the first discernable isophote. This procedure assumes that the light distribution in the central region is similar to that

farther out. Although this is known to be false in the case of NGC 6166, because of its multiple nuclei (Minkowski 1961), the errors introduced can be no larger than 30 % as this amount of the total diaphragm intensity comes from the two constructed isophotes of NGC 6166 and the three added isophotes of NGC 6173.

The areas of the isophotes within the photoelectric aperture were measured by means of a planimeter. These areas in square millimetres were then converted to angular areas. The radial distance of each isophote was measured along each semi-major axis and from them, values of log R were computed. Measurements for each semi-major axis were needed as the program PROFIL calibrates each semi-major axis separately on a relative scale. The folded brightness profiles produced by AVERAGEALL were calibrated using an average of the isophotal radial distances, and the total isophotal areas. Using each log R, a value of log I was read from the stacked profile of the galaxy along the appropriate semi-axis. The log I values from each semi-axis were then converted to relative magnitudes:

$$m = -2.5 \log I$$

Since the standard magnitude within the entire aperture was known from photoelectric photometry, and the relative magnitudes of the isophotes available, the problem of finding the appropriate scaling factor to convert the

relative magnitudes to standard magnitudes was solved by the Newton-Raphson method of iteration:

$$b_{i+1} = b_i + \frac{f(b_i)}{f'(b_i)}$$

where b is the scaling factor, and

$$f(b) = -2.5 \log \left[\sum_{j=1}^{N} \left(a_j \cdot 10^{-\left(\frac{m_j+b}{2.5}\right)} \right) \right] - M_{ph}$$

where N is the number of isophotes within the aperture, m_j and a_j are respectively the relative magnitude and area of the j^{th} isophote. M_{ph} is the photometric magnitude. Thus:

$$b_{i+1} = b_i + \frac{2.5 \log \left[\sum_{j=1}^{N} \left(a_j \cdot 10^{-\left(\frac{m_j+b}{2.5}\right)} \right) \right] + M_{ph}}{\log e \cdot \ln \left[10 \sum_{j=1}^{N} a_j \right]}$$

The scaling factor b is the number in magnitudes which must be added to the relative magnitudes of the computer-generated profile to obtain a standard surface brightness $\mu(r)$. Thus:

$$\mu(r) = -2.5 \log I(r)$$

As each semi-major axis of a galaxy is stacked separately, it is also normalized separately, and possibly at a different value. Thus the scaling factor may be different for each semi-axis. Taking this into consideration, a scaling factor for each semi-axis was computed using the isophotal brightness obtained from that semi-axis alone. The comparison of these scaling factors should provide an indication of the internal accuracy of the calibration process, as the two axes of the resulting calibrated profiles should have the same surface brightness at the nucleus, and the sky brightness levels for both axes should be equal.

The program ITERATE (see Appendix E) was written to perform the iterations, computing the scaling factor b when given the isophotal areas and their corresponding relative magnitudes. Table II is a list of all scaling factors from ITERATE. References for the photometric data are also given.

4.2 Calibration by a Photographic Transfer Technique

To calibrate the brightness profiles of galaxies for which neither photometry nor isodensity tracings were available, a different approach was needed. The elliptical galaxies on the same plate as a program cD galaxy were calibrated in the following manner.

A plate was chosen having a relatively uniform sky

TABLE II

Direct Calibration from Photometry

(Columns 4 to 6 are in magnitudes per square arcsecond, column 3 in magnitudes)

GALAXY	APERTURE	V	SCALING FACTOR N	S	FOLDED	REFERENCE
A 401 cD	27.4	15.30	28.22	27.95	28.64	1
A 2029 cD	36.8	14.33	27.34	27.39	27.67	1
A 2052 cD	48.3	13.62	27.10	27.06	27.05	2
NGC 6166	60.0	12.90	26.41	26.57	26.53	2
NGC 6173	45.1	13.20	26.34	26.29	26.31	3

References:

1 Welch, this study

2 Sandage, A. (1972)

3 Peterson, J. (1970)

density (in all cases a 20 minute V plate), the profiles from which had been included in the stacking runs. Several points were chosen along each axis from the density tracing of the (previously calibrated) cD galaxy on this plate. The density above clear plate D_{cp}, and the radial distance in arcseconds were determined for each point. Using the stacked profile for this calibrated galaxy, the log I values were read off for the appropriate log R positions.

These same density values D_{cp}, were then located on the density tracing of the uncalibrated galaxy above the clear plate level. Radial distances for the positions of these densities were determined and converted to arcseconds. The values, in the form of log R, were used to find corresponding values of log I from the stacked profile of the uncalibrated galaxy.

Since these log I values originated from the same densities above clear plate for both the calibrated and uncalibrated galaxies, then these positions on their respective profiles should have the same total absolute intensity, and thus the same total surface brightness. Assuming the sky to be of uniform brightness, the surface brightness at these locations in the two galaxies should therefore be the same.

The differences Δlog I were calculated, in the sense of calibrated minus uncalibrated, for each D_{cp}. The

average values were added to the scaling factor of the calibrated galaxy to produce the scaling factor for the uncalibrated galaxy. It was arbitrarily decided to match the semi-axes having similar orientation (eg. log I (NE axis of the calibrated galaxy) minus log I (NW axis of the uncalibrated galaxy)), thus producing two calibrations for each galaxy- one for each of its semi-major axes. A typical range in Δlog I for all points on both axes of a galaxy was ± 0.07.

The Δlog I values from both axes were averaged together, then added to the average of the calibrated galaxy's scaling factors for each semi-axis. This result was then applied to the folded profile of the uncalibrated galaxy. Table III gives a list of the scaling factors determined in this manner, including the plate and the cD galaxy from which it was calibrated.

As a check on this photographic transfer method of calibration, two galaxies previously calibrated directly from photometry, were also calibrated by this technique. Using the cD galaxy in Abell 2029 as the known galaxy, a scaling factor was determined for the cD galaxy in Abell 2052 (both are in the same plate field). The difference between the value obtained from photometry and that calculated indirectly was approximately 0.5 magnitudes per square arcsecond too faint. A similar 0.5 magnitude per square

TABLE III

Indirect Calibration Using Photographic Transfer Method

(Columns 4 and 5 are in magnitudes per square arcsecond)

GALAXY	PLATE	CALB.GLXY	Δ log I	b
A 401 #1	PS 7135	A 401 cD	0.28	28.38
#2	7135	A 401 cD	0.07	28.16
#3	7135	A 401 cD	0.24	28.34
A 2052 cD	5736	A 2029 cD	0.19	27.56
A 29/52#5	5736	A 2029 cD	0.49	27.85
AC	5736	A 2029 cD	0.28	27.65
NGC 6146	5755	NGC 6166	0.17	26.67
NGC 6160	5755	NGC 6166	0.09	26.58
NGC 6173	5755	NGC 6166	0.29	26.78

arcsecond difference was also found between the photometric calibration and photographic transfer scaling factors for NGC 6173, using NGC 6166 as the known galaxy. Considering the assumptions made for this indirect calibration method (ie. assuming uniform sky brightness over the extent of the galaxies), this discrepancy is acceptable.

The level of the sky brightness on each profile was determined in the following manner. From the NO AVERAGE computer runs, the values of relative sky intensity for each semi-axis of each galaxy tracing in the stacking run were added to the increment in log I recorded in the appropriate stacking runs. This increment is just the amount that tracing had to be shifted in log I to be stacked with the previous tracings. The average of these values for their respective axis or folded profile was then converted to a magnitude and added to the appropriate scaling factor, producing the average sky brightness of the tracings in the stacking run.

5.) RESULTS

5.1 Comparison with Published Results

The final calibrated surface brightness profiles are shown in Figures 1 through 21. These profiles have not been smoothed. Each point on the graphs represents the binned average of the data points processed from the tracings. "Noise" present in the faint outer regions is due to field objects (identified on the graphs), or to incomplete cancelation of random variations in sky fog. All graphs, with the exception of NGC 4881 (Figure 1), are absolute surface brightness, $\mu(r)$ in magnitudes per square arcsecond, versus log R in arcseconds. NGC 4881 was not calibrated since it was chosen as a check on the reduction process. The ordinate in Figure 1 was arbitrarily scaled in surface brightness:

$$s = 10 - 2.5 \log I$$

in magnitudes per square arcsecond.

a) NGC 4881

Figure 1 shows the data points produced from the present study (closed circles) using the AVERAGEALL option of PROFIL (ie. a folded profile). Also on the same graph, with its curve moved vertically in brightness to produce the best fit, is Strom and Strom's (1978a) data from the R bandpass (the

FIGURE 1: Arbitrarily scaled surface brightness s, of the giant elliptical galaxy NGC 4881. Dots (•) indicate data from this study, X's are the R bandpass data of Strom and Strom (1978a).

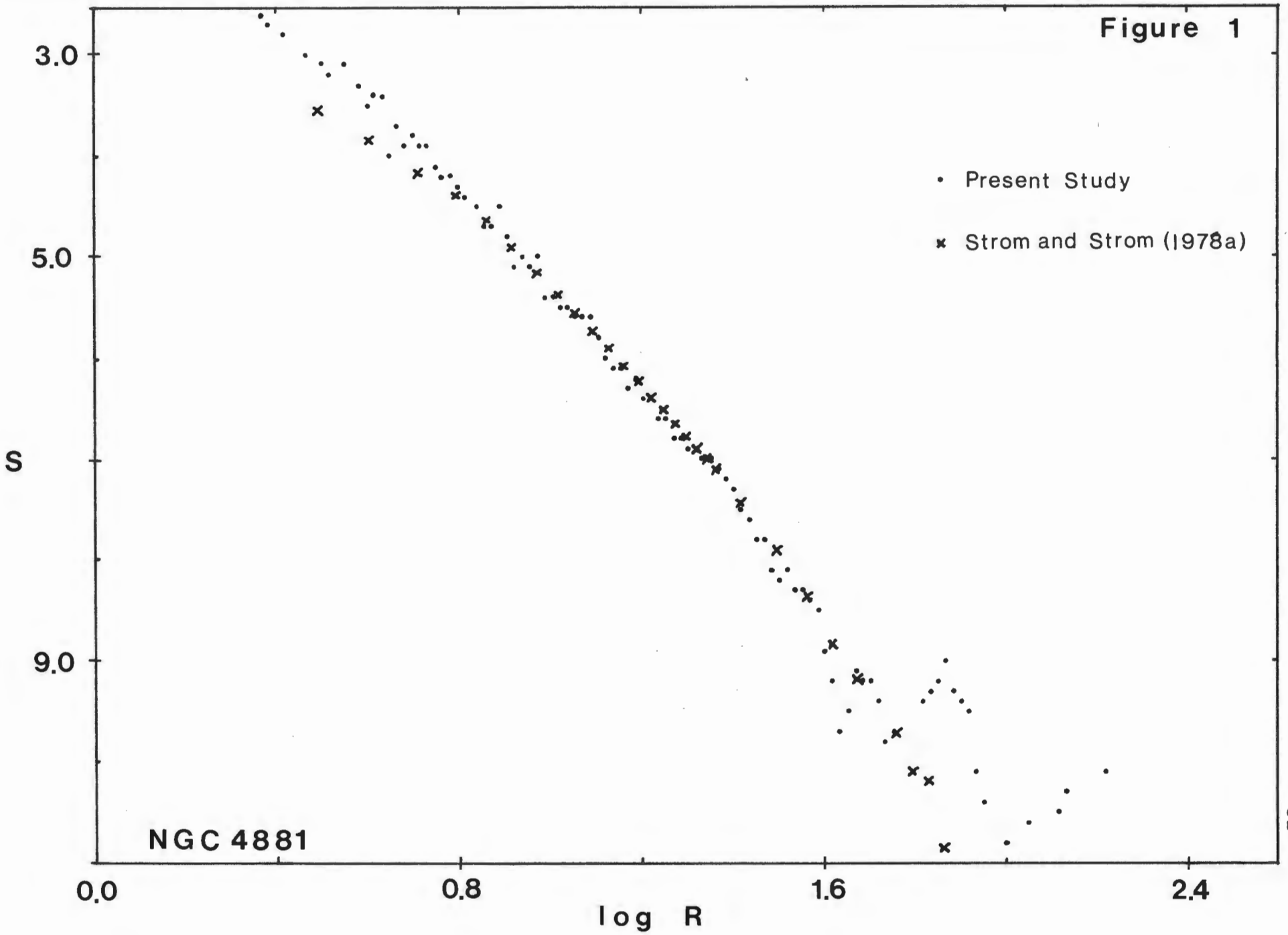
Figure 1
3.0
5.0
9.0
S
• Present Study
× Strom and Strom (1978a)
NGC 4881
0.0
0.8
1.6
2.4
log R

X's). It is easily seen that there is very good agreement between $0.8 \lesssim \log R \gtrsim 1.6$, with small discrepancies (~ 0.20) arising only within R = 5". Beyond log R $\sim$1.6, the details of the present tracings are lost in the noise. This indicates that the reduction process does not significantly distort the shape of a galaxy brightness profile.

b) NGC 6166

To test the calibration process used in this study, the averaged profile of the two semi-major axes of NGC 6166 was compared to the published J profiles of Carter (1977) and Oemler's (1976) profile in V. Table IV shows the surface brightnesses of the three studies at given arbitrary values of R, and their differences, Δ, at these points with respect to the present study, in the sense of this study minus the literature profile. It should be noted that the values from the literature are estimates taken from graphs included in the papers, and, at best, are accurate to approximately ± 0.15 magnitudes per square arcsecond for Carter, and ± 0.25 magnitudes per square arcsecond for Oemler.

The large discrepancies from Carter's results may be due in part to the artificially flattened profile near the nucleus, due, he states, to plate or microdensitometer saturation. Calibration difficulties also exist in Carter's profile. The depression of the profile amounts to a

TABLE IV

NGC 6166: Comparison with Published Results

(Columns 2 to 6 are in magnitudes per square arcsecond)

THIS STUDY		CARTER	Δ	OEMLER	Δ
R"	μ	(J)		(V)	
10.0	20.42	20.9	-0.48	20.8	-0.38
17.3	21.36	22.0	-0.64	21.8	-0.44
31.4	22.62	22.8	-0.18	23.1	-0.47
63.9	23.70	23.8	-0.10	24.4	-0.70
100.0	24.70	24.5	0.20	25.0	-0.30
sky	22.12	22.3	-0.18	---	---

difference of -1.8 magnitudes per square arcsecond at R = 2" with respect to the present study (Figure 21). A difference of only -0.18 magnitudes per square arcsecond in the sky brightness levels semms to support the argument that there is a problem in the inner portions of the curve, as it agrees closely with the smaller deviations between the points chosen at greater distances along the curves. Carter does not indicate, however, the exact extent of the saturation effects.

Discrepancies with respect to Oemler's profile may be a result of his choosing a different position for the nucleus of the galaxy, because of its multiple structure in the central region. At R = 2.5" the difference in brightness is approximately -0.3 magnitudes per square arcsecond; no sky brightness is given.

Some systematic error is possible in the calibration as the present profile seems too bright by 0.2 to 0.5 magnitudes per square arcsecond with respect to the published profiles. However, the profiles should be expected to agree only if they represent the same path through the galaxy (with the exception of agreement at the nucleus and of the sky brightness). The present profile is the average of the profiles through the two semi-major axes, while Carter uses a method of averaging points along radial arcs which subtend a constant angle ($\sim 45^{\circ}$). This variation in technique and the existance of multiple nuclei could very well explain the large discrepancy

between the two profiles near the nucleus of NGC 6166. Oemler's reduction method uses a similar approach, except that approximately 50 points along assumed concentric elliptical isophotes are used.

Systematic magnitude differences between the profiles in the present study and those of Carter are expected, as different photometric systems were used for calibration. Carter's profiles were calibrated using the blue-green J bandpass, while the present study utilized the V bandpass. Oemler (1973) gives the relation between these systems as V - J = -0.3 magnitudes for the inner 10" of the cD galaxy in Abell 2670, on the same order as the recorded differences.

c) NGC 6146, 6160, and 6173

Table V gives the comparisons of the results of the present study to those of Carter (1977) for the elliptical galaxies NGC 6146, 6160, and 6173, all of which were on the same plate as NGC 6166 and were calibrated from it (NGC 6173 was also calibrated directly, using photoelectric photometry. See section 4.2). Differences are again in the sense of present study minus Carter's values.

The mean differences for NGC 6173 and 6160 are approximately on the order, and in the sense of, the values expected due to the bandpass difference. In NGC 6146, however, the sense of the differences is incorrect. This discrepancy

TABLE V

Comparison of Results with those of Carter (1977)

(Columns 2 to 4 are in magnitudes per square arcsecond)

THIS STUDY		CARTER	DIFFERENCE
R"	μ	(J)	
NGC 6146			
10.0	21.52	21.6	-0.08
17.8	22.61	22.5	0.11
31.61	24.06	23.7	0.36
100.0	26.72	26.4	0.32
sky	22.72	22.35	0.37
NGC 6160			
10.0	21.56	21.9	-0.34
17.8	22.37	22.7	-0.33
31.6	23.38	23.5	-0.12
100.0	25.84	25.5	0.34
sky	22.37	22.35	0.02
NGC 6173			
10.0	21.33	21.8	-0.47
17.8	22.44	22.7	-0.26
31.6	23.54	23.8	-0.26
100.0	25.78	26.0	-0.22
sky	22.86	22.35	0.51

could be caused by the choice of sky level.

d) Conclusions

Based on the comparisons with the published brightness profiles of Strom and Strom, and Oemler, there appears to be no evidence for spurious brightness gradients larger than 0.002 magnitudes per square arcsecond per arcsecond over the brightness range $22.5 \lesssim \mu(R) \lesssim 24.5$ magnitudes per square arcsecond. There does seem to be a systematic difference of approximately -0.4 magnitudes per square arcsecond in the calibration zero point with respect to Oemler's profile of NGC 6166. The reason for this could be the dissimilarity in calibration techniques.

Carter's photometry shows mean slope differences of 0.005 magnitudes per square arcsecond per arcsecond over $1.25 \lesssim \log R \lesssim 2.0$, the present study having the steeper slope, and the largest deviations occurring in NGC 6146 and 6160. This may indicate Carter's choice of a lower value for the sky density than was used in this study, making the slope of his curve shallower. Evidence for this possibility is reflected in the fact that the discrepancies near the nucleus are on the order expected by the bandpass difference. Saturation near the nucleus of Carter's profile of NGC 6166 may be responsible for the relatively large slope difference of 0.010 magnitudes per square arcsecond per arcsecond.

5.2 The Elliptical Galaxies

The elliptical galaxies in this study were originally chosen because of their appearance as typical elliptical galaxies, from examination of deep V plates taken with the 1.2m (48 inch) Schmidt telescope. Their purpose was to confirm that the reduction procedures yield reasonable results for standard objects.

In all cases the profiles were fit to de Vaucouleurs' (1953) law for elliptical galaxies:

$$\log \frac{I}{I_\circ} = -3.33 \left[\left(\frac{R}{R_\circ} \right)^{1/4} - 1 \right]$$

where $R_\circ$ is the radius (in seconds of arc) at which the intensity $I_\circ$ is one half the central value. This relation seems to describe their shape very well. It does not, however, represent the inner regions of standard elliptical galaxies, so agreement near R = 0 is not expected.

Two other relations were also tried; the empirical King (1962) formula:

$$f = k \left[\frac{1}{\left(1 + \left(\frac{R}{R_c} \right)^2 \right)^{1/2}} - \frac{1}{\left(1 + \left(\frac{R_t}{R_c} \right)^2 \right)^{1/2}} \right]^2$$

where R_t is the tidal radius, R_c is the core radius, and k is a constant; and Oemler's (1976) reduced Hubble law:

$$S = \frac{I_o \exp\left[-\left(\frac{R}{\alpha}\right)^2\right]}{(R + \beta)^2}$$

where S is the intensity at radius R, and I_o is the reduced luminousity, and α and β are fitting parameters. The King formula fit the outer portions of the galaxy profiles well, but tended to predict much fainter inner regions than were observed. The fitting of the reduced Hubble law to the program ellipticals produced no improvement over the de Vaucouleurs relation.

For the fitting procedure, two points were arbitrarily chosen along the profile. The choice of points was then changed until a best fit of the relation to the profile was achieved. Arrows marked by V's denote the final choice of fitting points.

A-401 #1

The folded brightness profile of the elliptical galaxy identified as #1 (Figure 2) on the plate containing the cluster Abell 401, displays a good fit to the de Vaucouleurs law beyond log R = 0.4. The scatter about the curve is small, ±0.10, and no cutt-off in the profile is visible to approximately 27.5 magnitudes per square arcsecond. An abrupt cut-off in the profile would indicate the possibility that the sky level on the plate had been chosen too bright.

FIGURE 2: Folded axes surface brightness profile of the elliptical galaxy #1 in the plate field of Abell 401. "a" indicates the position where light is introduced into the profile by a foreground star on the S axis.

On this and all other graphs, the V's indicate the points used to fit de Vaucouleurs' law (1953) to the profile. The surface brightness $\mu(r)$ is in magnitudes per square arcsecond; R is in arcseconds. The line labelled "sky" is the sky brightness level.

FIGURE 3: Folded axes surface brightness profile of the elliptical galaxy #2 in the plate field of Abell 401.

FIGURE 4: Folded axes surface brightness profile of the elliptical galaxy #3 in the plate field of Abell 401.

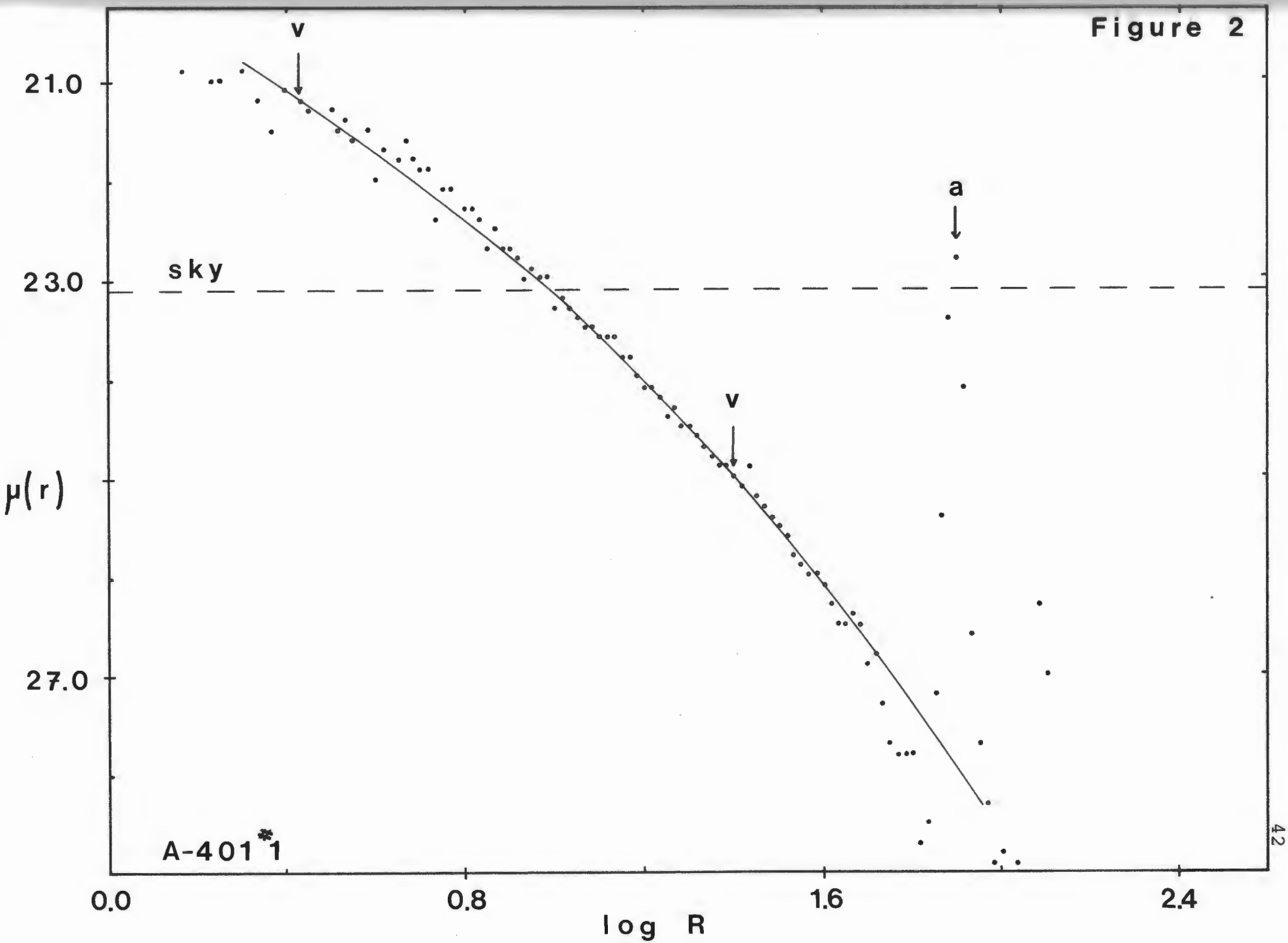
Figure 2
v
a
v
sky
21.0
23.0
27.0
μ(r)
A-401 *1
0.0
0.8
1.6
2.4
log R
42

Figure 3

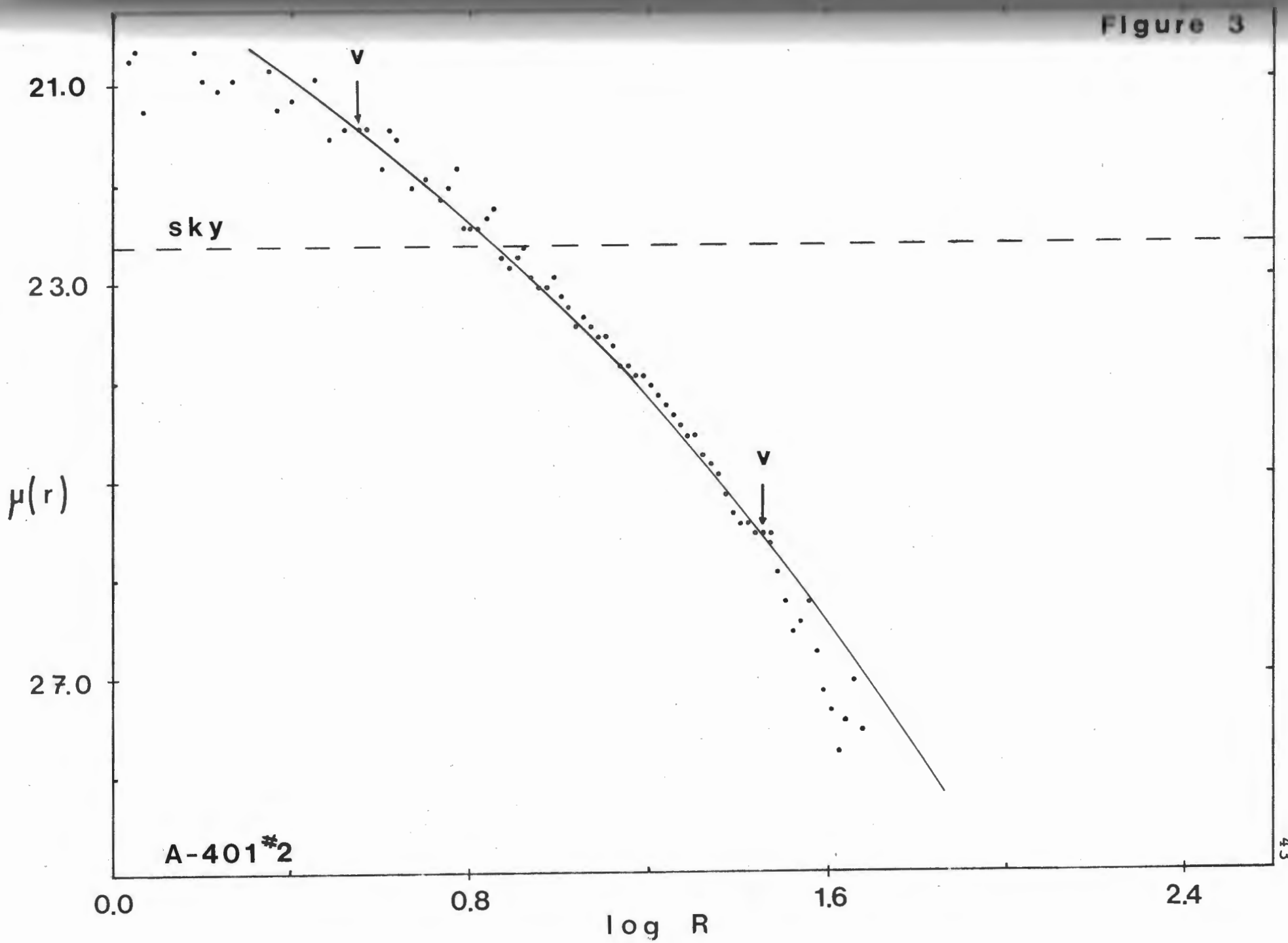

Figure 4

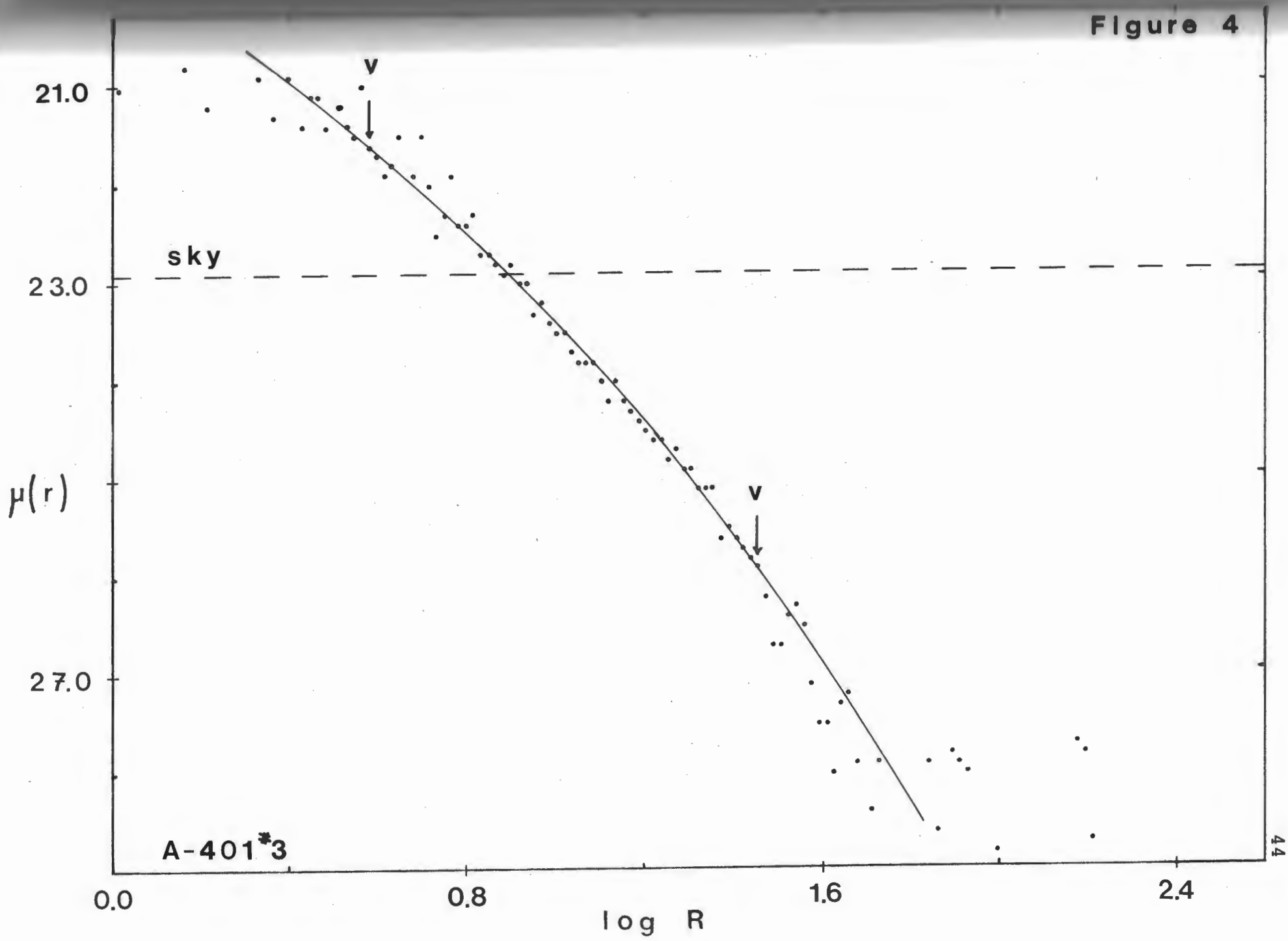

A-401 #2

Figure 3 gives the brightness profile of the folded axes of galaxy #2. The scatter near the nucleus is moderate, ±0.23, and is probably caused by its asymmetric axes. The tracings from PS 7168 (a 20 minute 103a-D plate) on the SW axis and PS 7169 (a 2 hour IIIa-J plate) on the NE axis are brighter than the average of the other tracings. Otherwise, the rest of the profiles fit the de Vaucouleurs law well.

A-401 #3

Figure 4 shows the folded axes surface brightness profile of the elliptical galaxy #3. The profile fits the de Vaucouleurs relation well. There is scatter (±0.23) near the nucleus introduced by the 20 minute V plate PS 7168 along the NW axis, it being slightly brighter than the average of the other three tracings.

A-29/52 #5

The brightness profile of galaxy #5 in the field of the clusters Abell 2029 and 2052 is shown in Figure 5. It produces a good fit with the de Vaucouleurs relation with very little scatter (±0.10), except around log R = 0.3, where there is asymmetry in the two axes. No cut-off of the profile is noticeable to 27.0 magnitudes per square arcsecond, where a foreground star obscures the profile of the outer regions of the galaxy.

A-29/52 AC

This galaxy has a very interesting surface brightness profile (Figure 6). Although classified as an S0 from a V plate by Dr. Welch when picked for this study, later examination of its image on the IIIa-J plates revealed that it does not possess the typical S0 halo, but seems to have an extended halo, similar in appearance to those of giant elliptical and supergiant galaxies. This observation is consistent with the appearance of its brightness profile. It is nearly linear on the $\mu(R)$ versus log R plot and in fact, with a slope of -3.94, fits the Bahcall relation very well. Departure from de Vaucouleurs' law is small until log R $\sim$ 1.7, beyond which the predicted brightness for an elliptical galaxy declines more rapidly than the light of AC.

Since formation of a cD-type extended halo is at present explained by interactions within a cluster of galaxies, the IIIa-J plates of this region were examined for possible cluster membership. Several fainter galaxies are located within 20' of AC, but no evidence of a clustering about the galaxy was found. Neither Abell (1958) nor Zwicky et al. (1961-68) list a cluster in this area, although the field within $\sim 4^{\circ}$ is well populated with galaxies. The closest galaxy of comparable luminosity is an elliptical galaxy approximately 11' south of AC. No other galaxy of similar brightness is within 25'.

FIGURE 5: Folded axes surface brightness profile of the elliptical galaxy #5 in the plate field of Abell 2029 and 2052. "a" indicates the position of light from a foreground star on the NW axis.

FIGURE 6: Folded axes surface brightness profile of the galaxy AC in the plate field of Abell 2029 and 2052. "a" is the position of a foreground star on the SE axis. "b" is the light from another galaxy superimposed on the NW axis profile. "c" is a foregroud star on the NW axis.

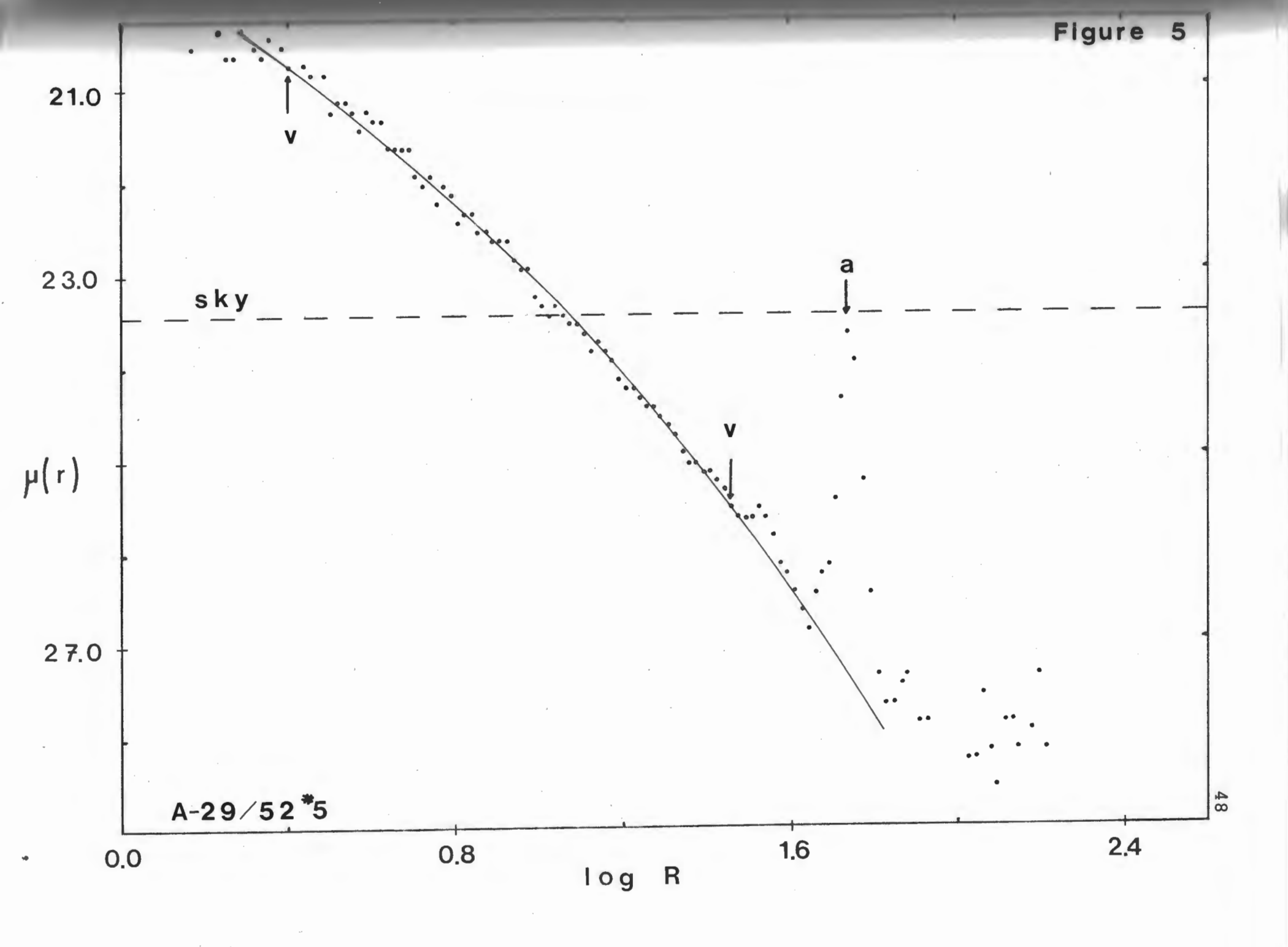
Figure 5
21.0
23.0
27.0
μ(r)
sky
v
v
a
A-29/52*5
0.0
0.8
1.6
2.4
log R
48

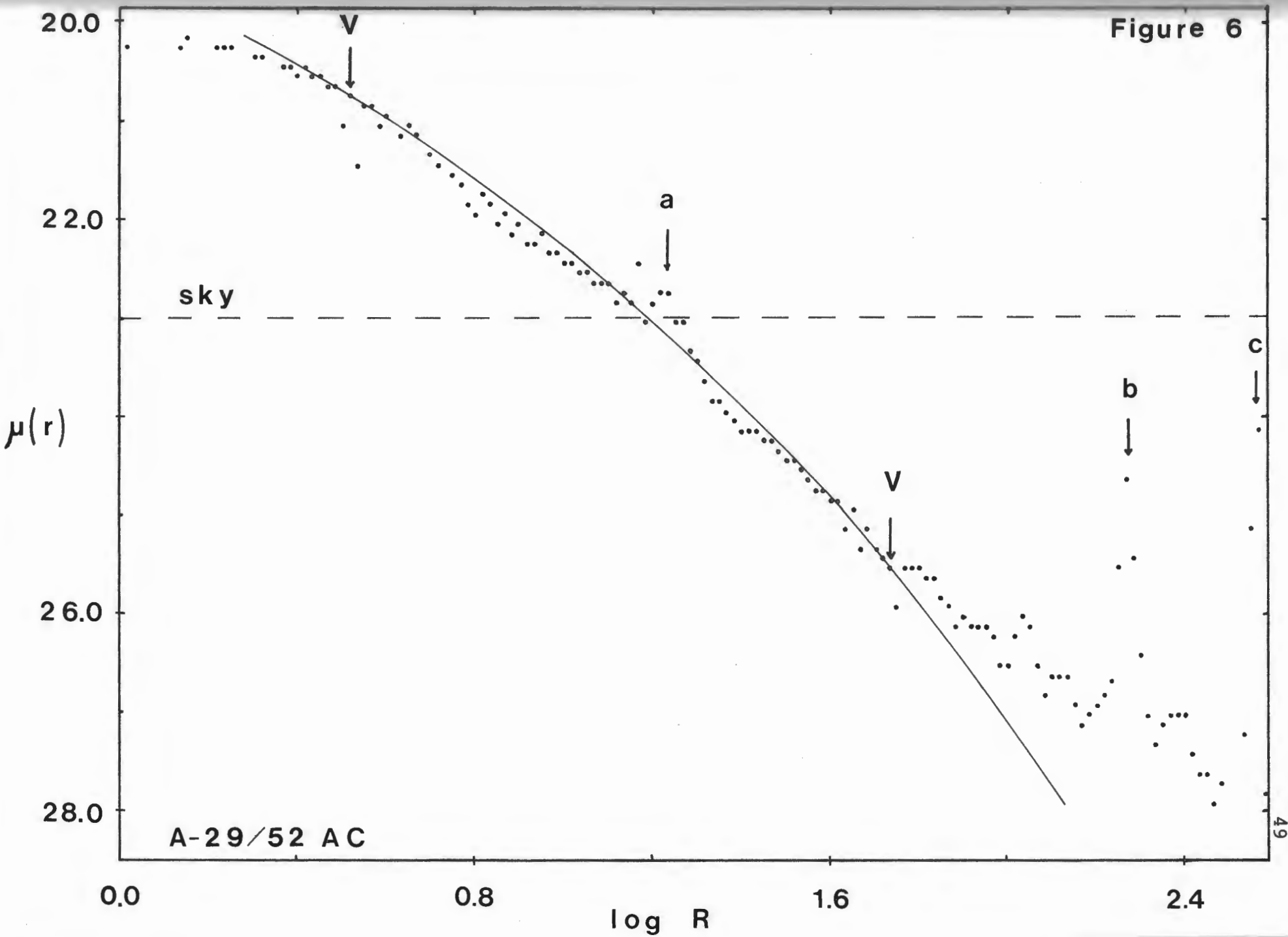
Figure 6
20.0
22.0
26.0
28.0
μ(r)
V
a
sky
V
b
c
A-29/52 AC
0.0
0.8
1.6
2.4
log R

No radial velocity could be found for this galaxy, so its actual size and distance are unknown. It could be either a small, relatively nearby field galaxy, or a large, distant cD or giant elliptical galaxy, possibly in a poor cluster. The implications which arise from the appearance of AC's light distribution will be discussed later.

NGC 6146

The average of the two axes of the E2-3 galaxy NGC 6146 is shown in Figure 7. Its profile is quite smooth from approximately log R = 0.9 to log R = 1.6, and follows the de Vaucouleurs relation well in this interval. Beyond log R $\sim$ 1.6, field objects make it difficult to determine the true light distribution. This galaxy, with NGC 6160 and 6173, are members of Abell 2197, a rich cluster physically close to Abell 2199 (which contains the cD galaxy NGC 6166).

NGC 6160

Figure 8, the folded profile of the E2 galaxy NGC 6160, is a good fit to the de Vaucouleurs law. It contains slightly more scatter along the outer portion of the curve than #1, #2, and #5, but fits well towards the nucleus, where the deviation from the curve is ±0.14.

FIGURE 7: Folded axes surface brightness profile of the elliptical galaxy NGC 6146. "a" is the position of a foreground star on the NE axis. "b" is the position of a foreground star on the SW axis.

FIGURE 8: Folded axes surface brightness profile of the elliptical galaxy NGC 6160.

FIGURE 9: Folded axes surface brightness profile of the giant elliptical galaxy NGC 6173. "a" is the position of another galaxy superimposed on the profile of the N axis.

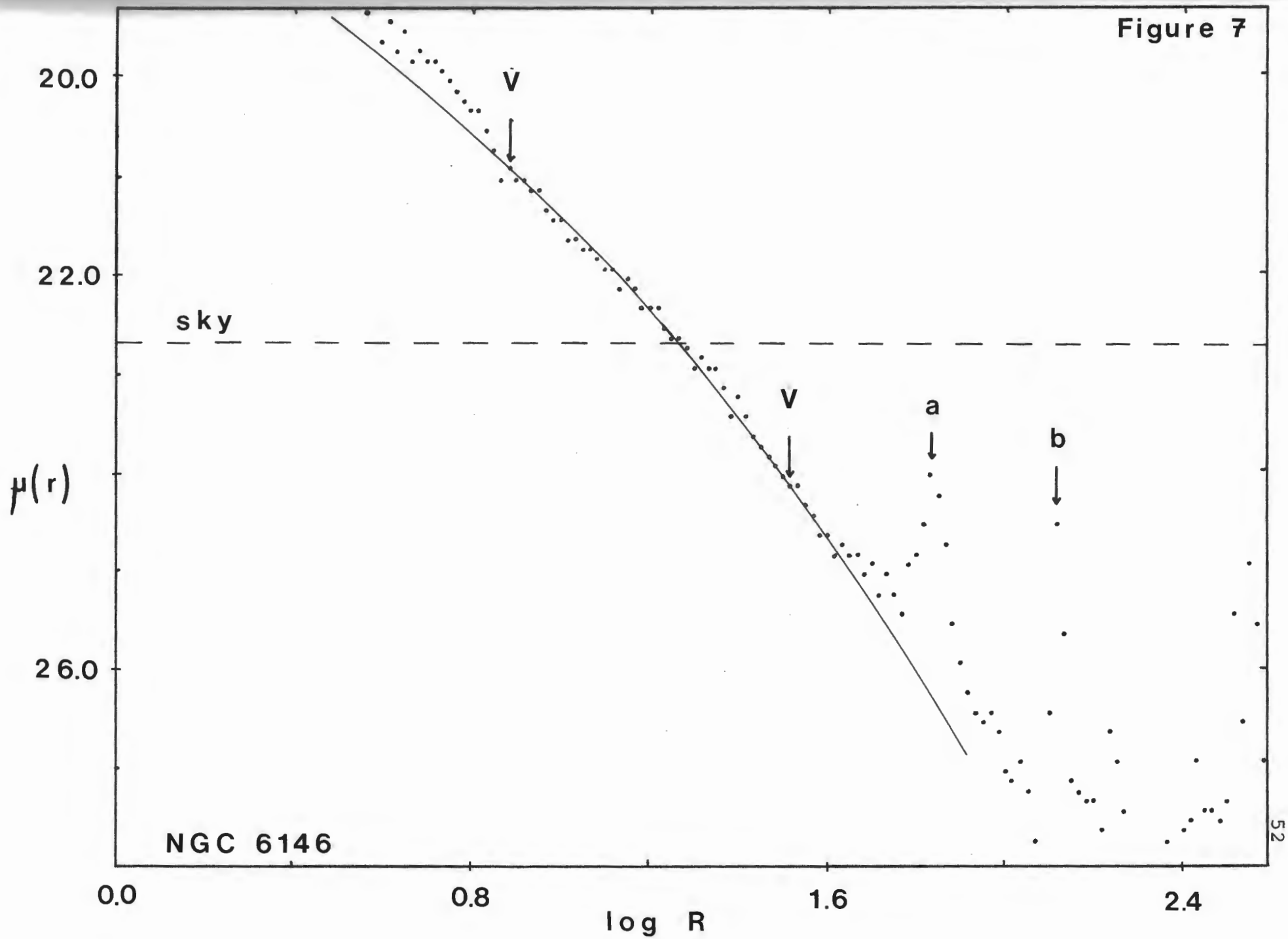
Figure 7
20.0
22.0
sky
26.0
μ(r)
V
V
a
b
NGC 6146
0.0
0.8
1.6
2.4
log R

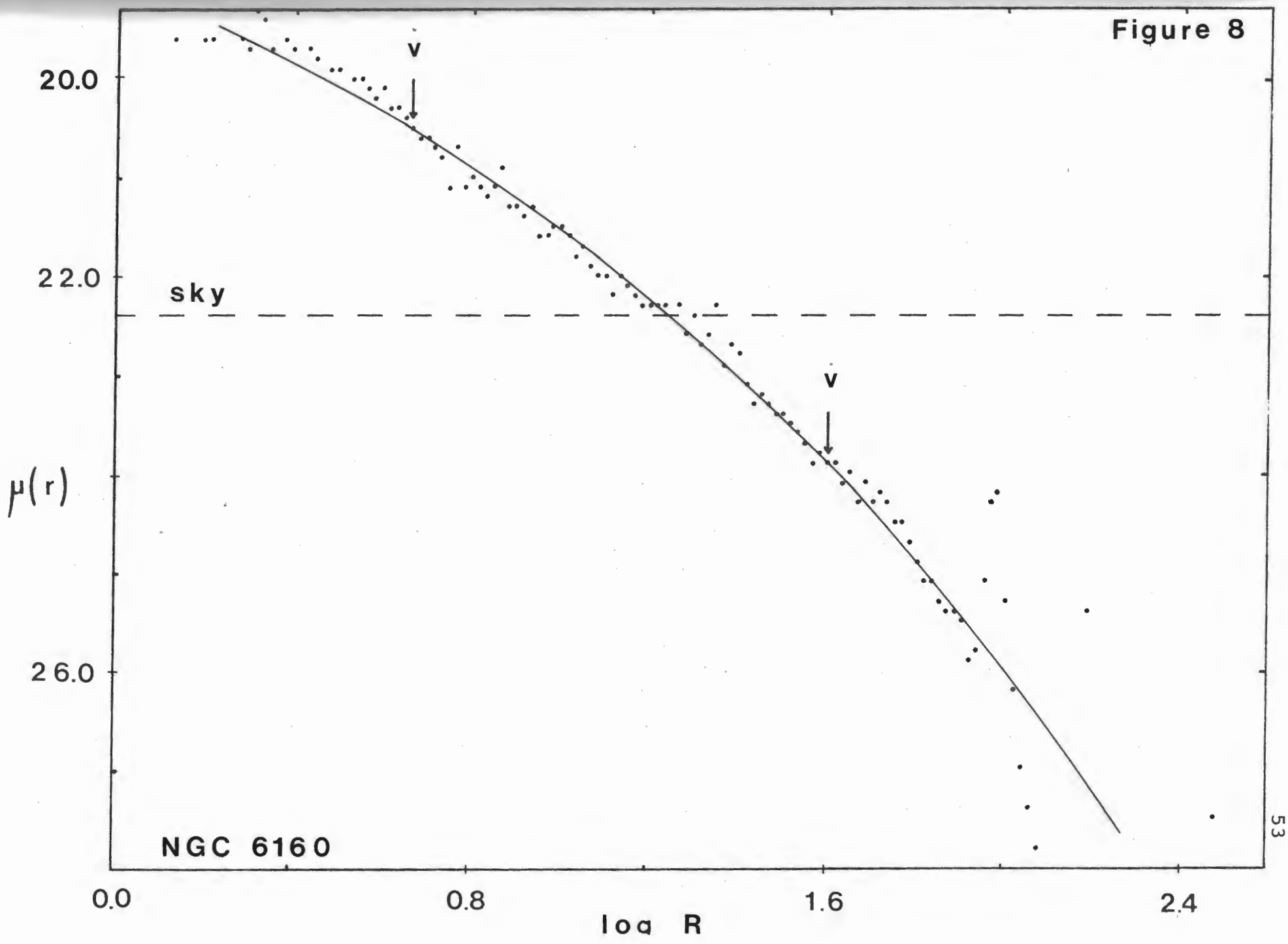
Figure 8
20.0
22.0
26.0
sky
v
v
μ(r)
NGC 6160
0.0
0.8
1.6
2.4
log R

Figure 9

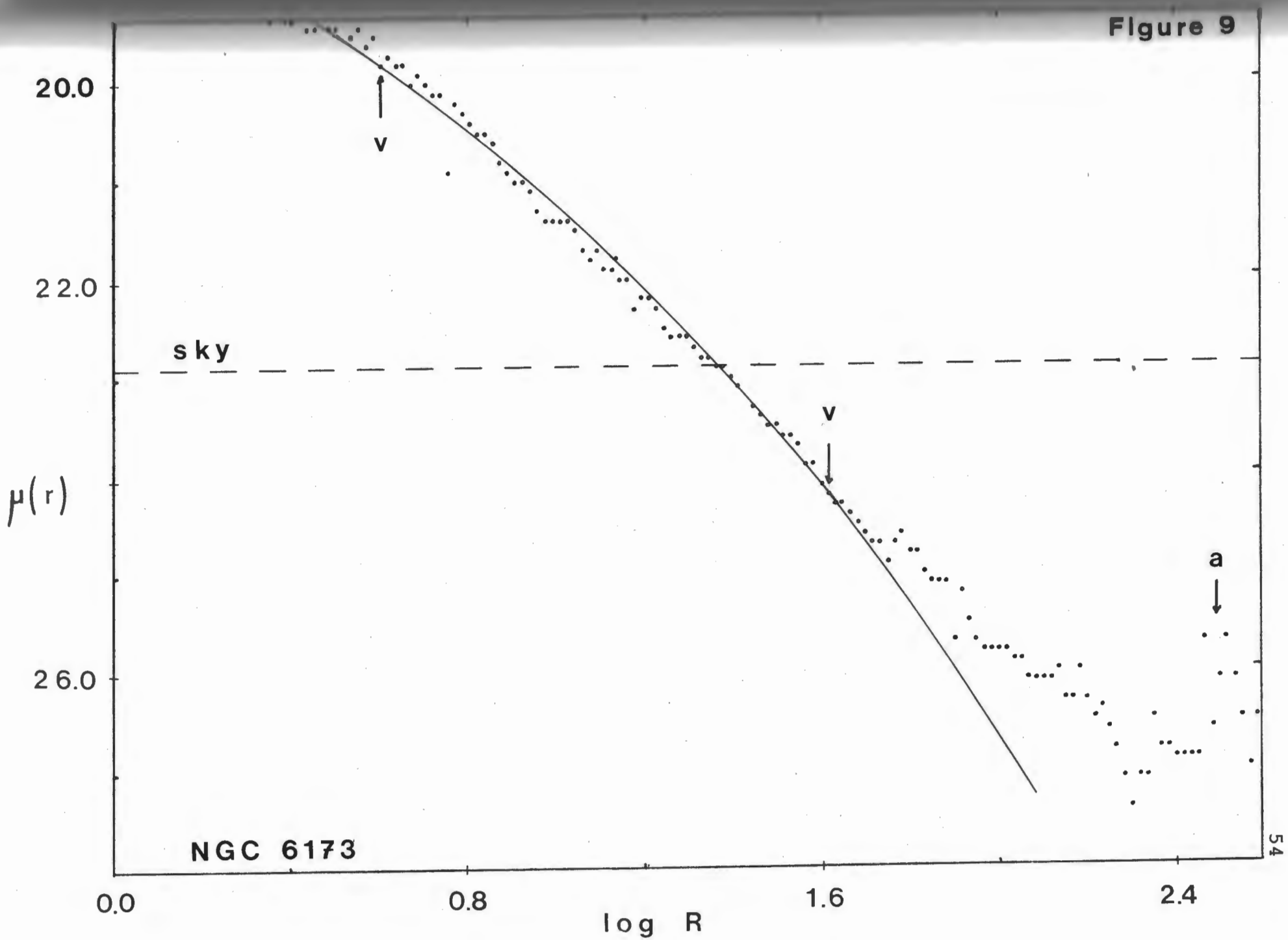

NGC 6173

Figure 9 gives the surface brightness profile of the averaged axes of the giant elliptical NGC 6173. It fits the de Vaucouleurs law well (scatter about the curve is only ±0.12) until about log R ∿ 1.6, then the profile gradually becomes brighter than is expected for a normal elliptical galaxy. This exponential behavior of the light distribution is typical of giant ellipticals. Its profile is much steeper (slope = -4.50) however, than Bahcall's slope of -4.00 for supergiant galaxies. NGC 6173 is the brightest cluster gal. galaxy of Abell 2197.

5.3 The Supergiant Galaxies

The cD galaxies in this study were fit to both the de Vaucouleurs law and to the Bahcall relation:

$$I(R) \propto R^{-1.6}$$

where I is the intensity at radial distance R. The fitting procedure for the de Vaucouleurs law was the same as was used for the elliptical galaxies (ie. solving for two points), but the Bahcall relation was moved in $\mu(R)$ until a satisfactory fit was obtained.

Abell 401 cD

The supergiant galaxy in the cluster Abell 401 (Figures 10, 11, and 12) presents a different profile than the other cD galaxies in this program. The profile is noticeably flatter throughout its length, with none of the leveling off near the nucleus, seen in the profiles of the other program galaxies. While it is difficult to be certain due to numerous field objects which contribute to the light beyond log R ≈ 1.8, there appears to be no abrupt decline in surface brightness.

The mean slope of the folded profile (Figure 12) beyond log R ∿ 0.5 is -2.75, considerably flatter than the value of -4.00 suggested by Bahcall. In fact, even within log R = 1.6, where the profile should not be significantly affected by field objects, the slope is -2.45.

The profile does fit the de Vaucouleurs law for elliptical galaxies quite well to log R ∿ 1.6, however, at greater distances, the brightness declines much less rapidly than the normal elliptical galaxy. This is seen more readily in the profile of the SW axis, as the NE axis is affected by several other cluster members.

Abell 2029 cD

Figures 13, 14, and 15 represent the N axis, S axis, and folded axes surface brightness profiles of the cD galaxy in Abell 2029. Its profile appears brighter than that

FIGURE 10: Surface brightness profile of the NE axis of the cD galaxy in Abell 401. "a" and "b" are the positions of other galaxies superimposed on the profile of this axis. "c" is the position of a foreground star.

FIGURE 11: Surface brightness profile of the SW axis of the cD galaxy in Abell 401.

FIGURE 12: Folded axes surface brightness profile of the two semi-axes of the cD galaxy in Abell 401.

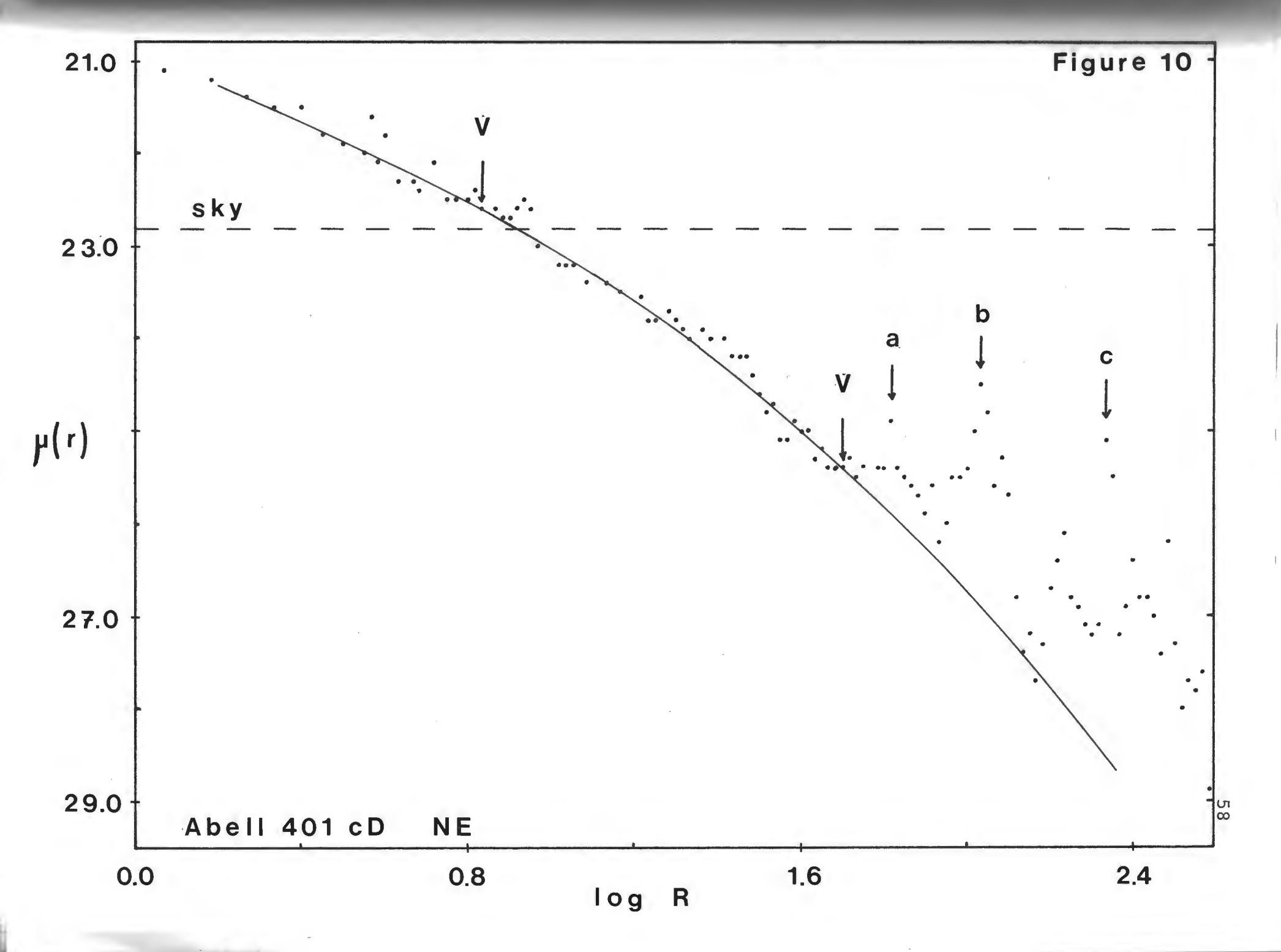
Figure 10
21.0
23.0
27.0
29.0
μ(r)
sky
V
V
a
b
c
Abell 401 cD NE
0.0
0.8
1.6
2.4
log R
58

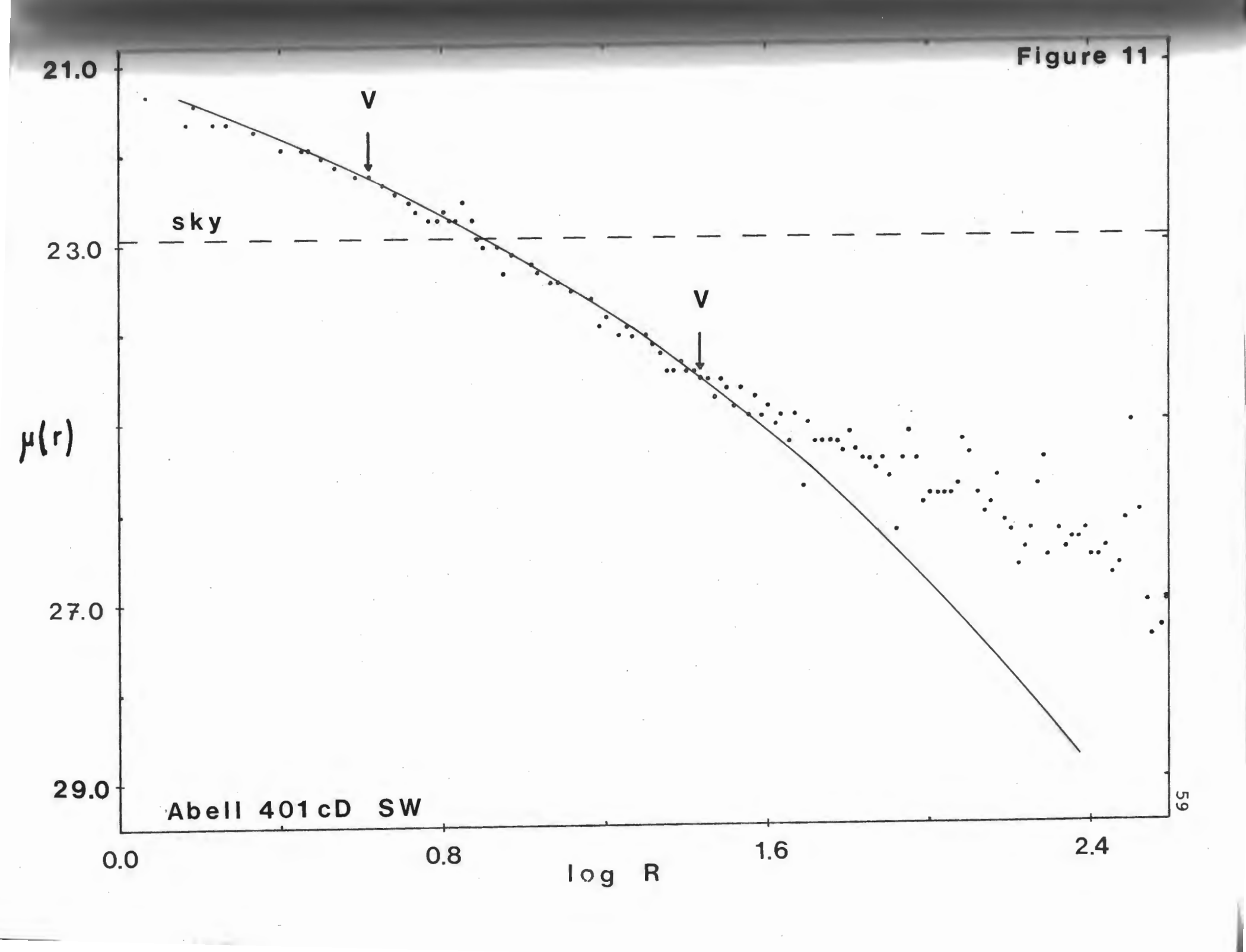
Figure 11
21.0
V
sky
23.0
V
μ(r)
27.0
29.0
Abell 401 cD SW
0.0
0.8
1.6
2.4
log R
59

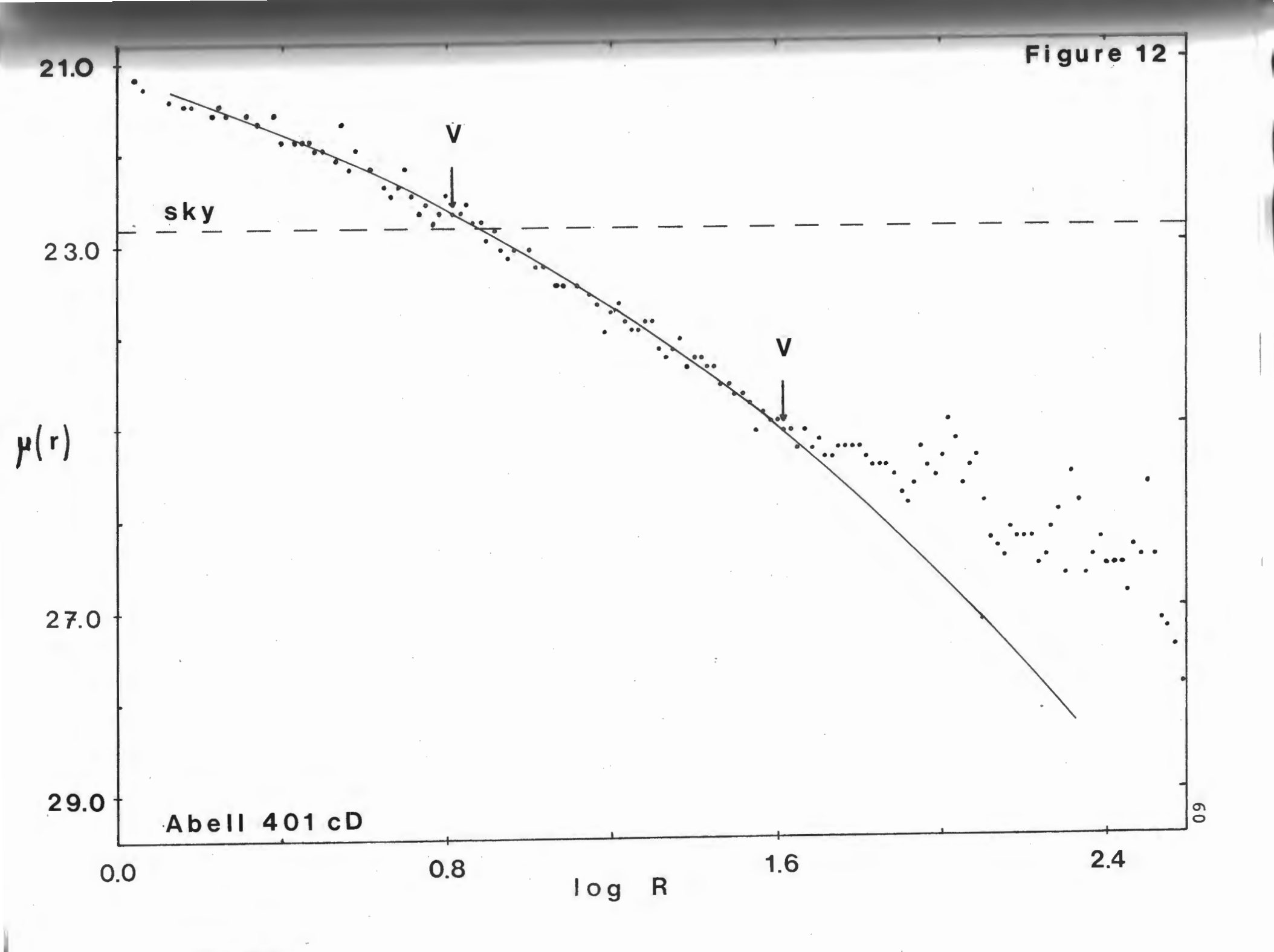
Figure 12
21.0
23.0
27.0
29.0
μ(r)
sky
V
V
Abell 401 cD
0.0
0.8
1.6
2.4
log R
60
09

FIGURE 13: Surface brightness profile of the N axis of the cD galaxy in Abell 2029. "a" and "b" are the positions of foreground stars. "c" is another galaxy superimposed on the profile of this axis.

FIGURE 14: Surface brightness profile of the S axis of the cD galaxy in Abell 2029. "a" and "c" are the positions of foreground stars. "b" is another galaxy superimposed on the profile of this axis.

FIGURE 15: Folded surface brightness profiles of the two semi-axes of the cD galaxy in Abell 2029.

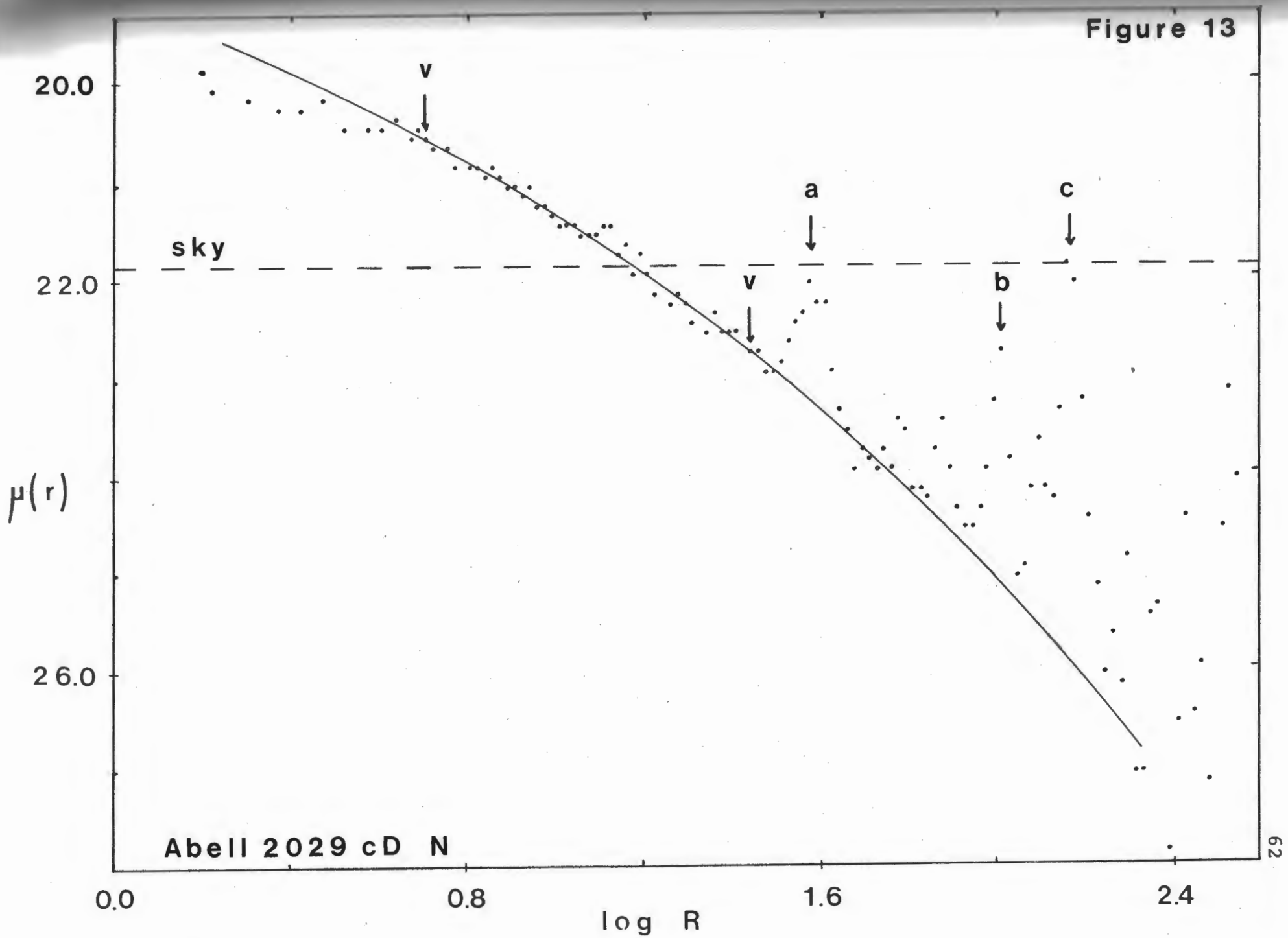
Figure 13
20.0
22.0
26.0
μ(r)
sky
v
v
a
b
c
Abell 2029 cD N
0.0
0.8
1.6
2.4
log R
62

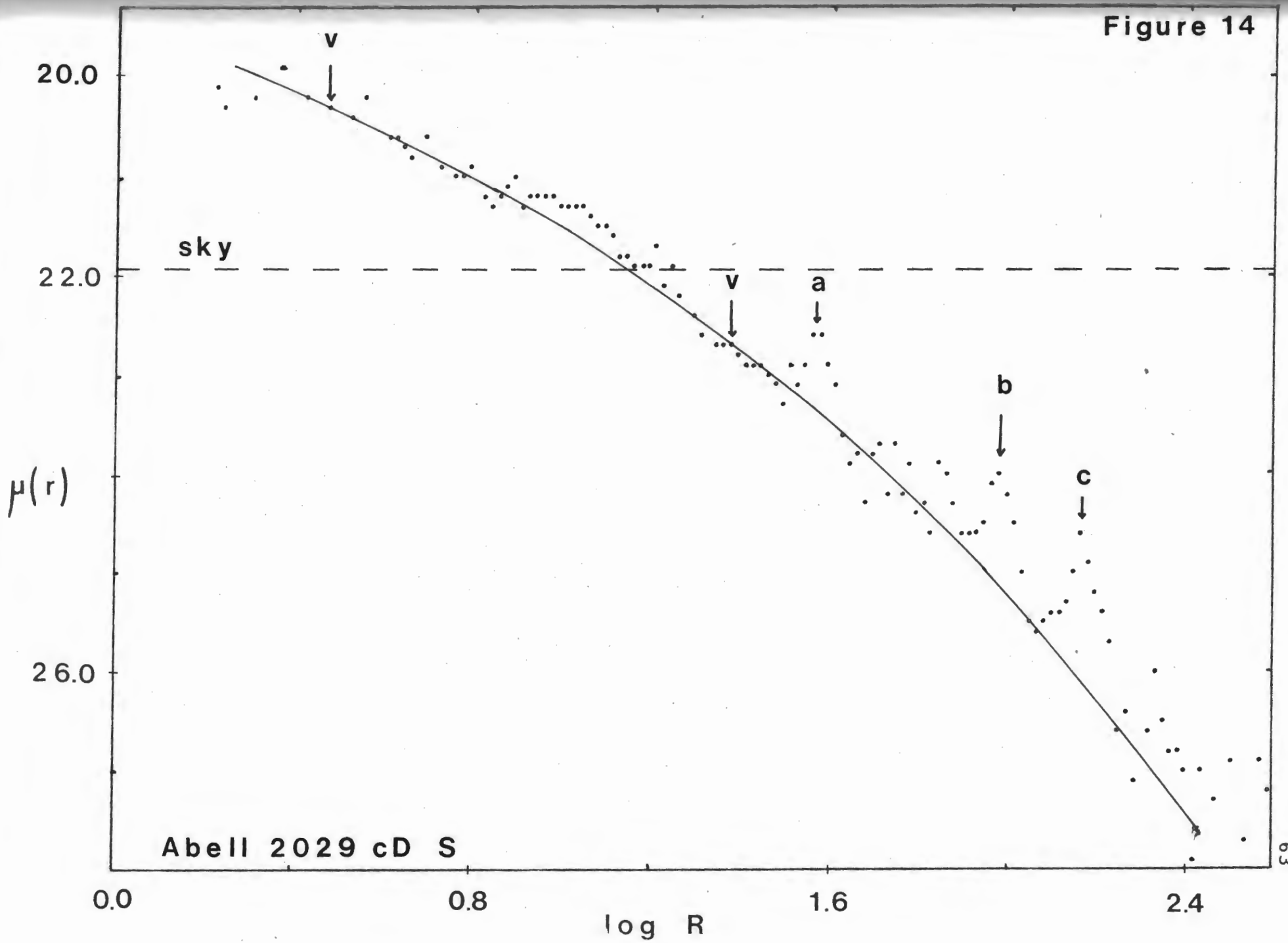
Figure 14
20.0
22.0
26.0
sky
v
v
a
b
c
μ(r)
Abell 2029 cD S
0.0
0.8
1.6
2.4
log R
63

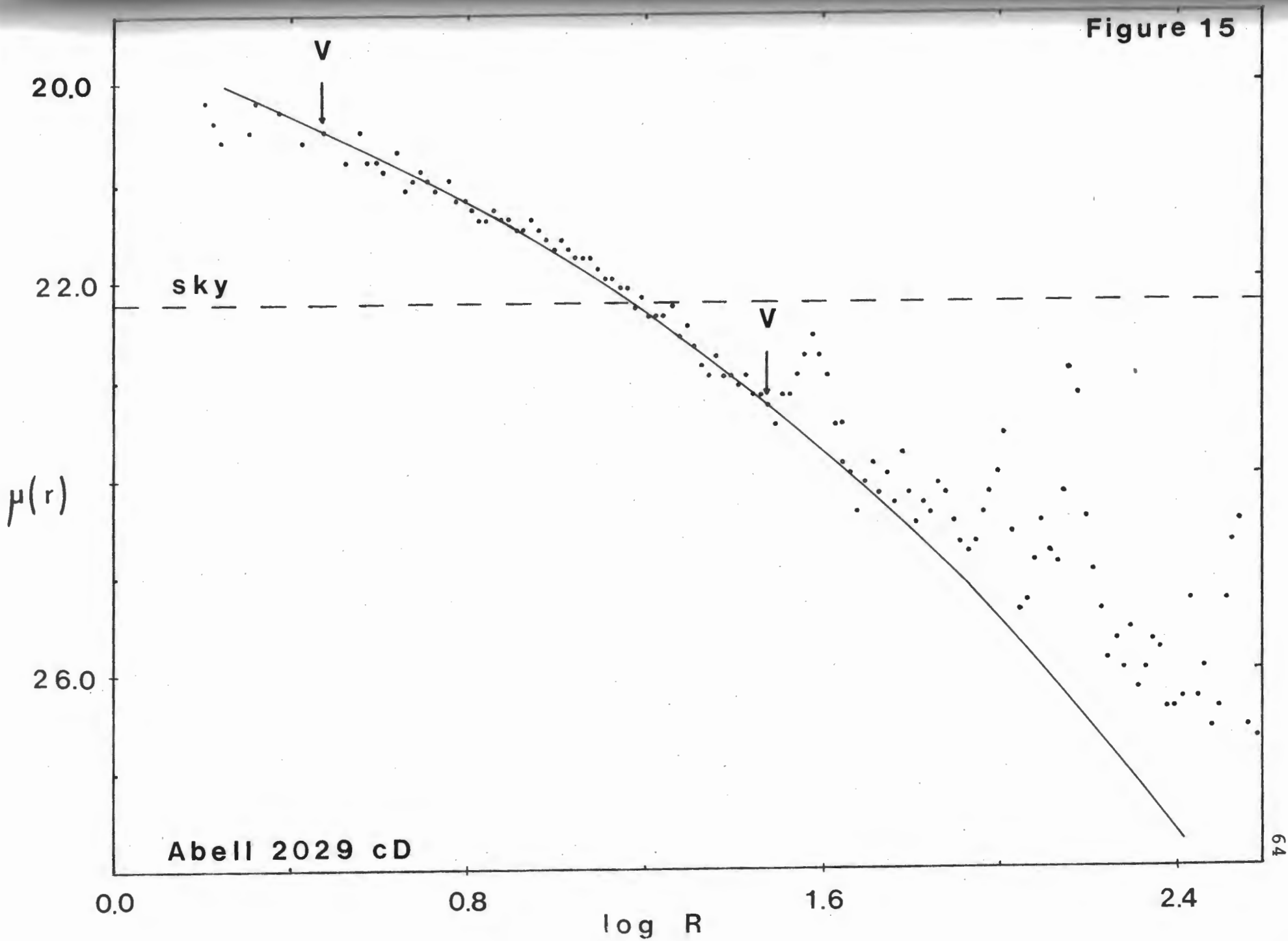
Figure 15
V
20.0
22.0
sky
V
μ(r)
26.0
Abell 2029 cD
0.0
0.8
1.6
2.4
log R
64

expected for a normal elliptical galaxy. However, due to the high density of cluster galaxies in the region of the cD galaxy, it is difficult to determine how much of their outer regions contribute to the cD profiles.

Using the S axis profile (Figure 14), as it is probably less influenced by other cluster members, a mean slope of -4.0 is obtained beyond log R = 0.9, as expected by the Bahcall relation.

Abell 2052 cD

The surface brightness profiles of the cD galaxy in Abell 2052 (Figures 16, 17, and 18) give very good fits to Bahcall's relation for $0.9 \lesssim \log R \lesssim 2.1$, with a slope of -4.0 for the folded axes profile (Figure 18). The large scatter in the folded profile near the nucleus is introduced by the SW axis, and is probably due to inaccurate positioning of the nucleus on one or more tracings (see discussion in sections 2.2 and 3.4). On short exposure plates, one of the two central condensations is seen slightly to the NE of centre. This asymmetry could account for the scatter within $\log R \sim 0.5$ in the folded profile.

NGC 6166

NGC 6166, shown in Figures 19, 20, and 21, is one of the archtypical cD galaxies (Matthews et al.). As can be

FIGURE 16: Surface brightness profile of the NE axis of the cD galaxy in Abell 2052.

FIGURE 17: Surface brightness profile of the SW axis of the cD galaxy in Abell 2052. "a" and "b" are the positions of foreground stars. "c" is another galaxy superimposed on the semi-axis profile.

FIGURE 18: Folded axes surface brightness profile of the two semi-axes of the cD galaxy in Abell 2052.

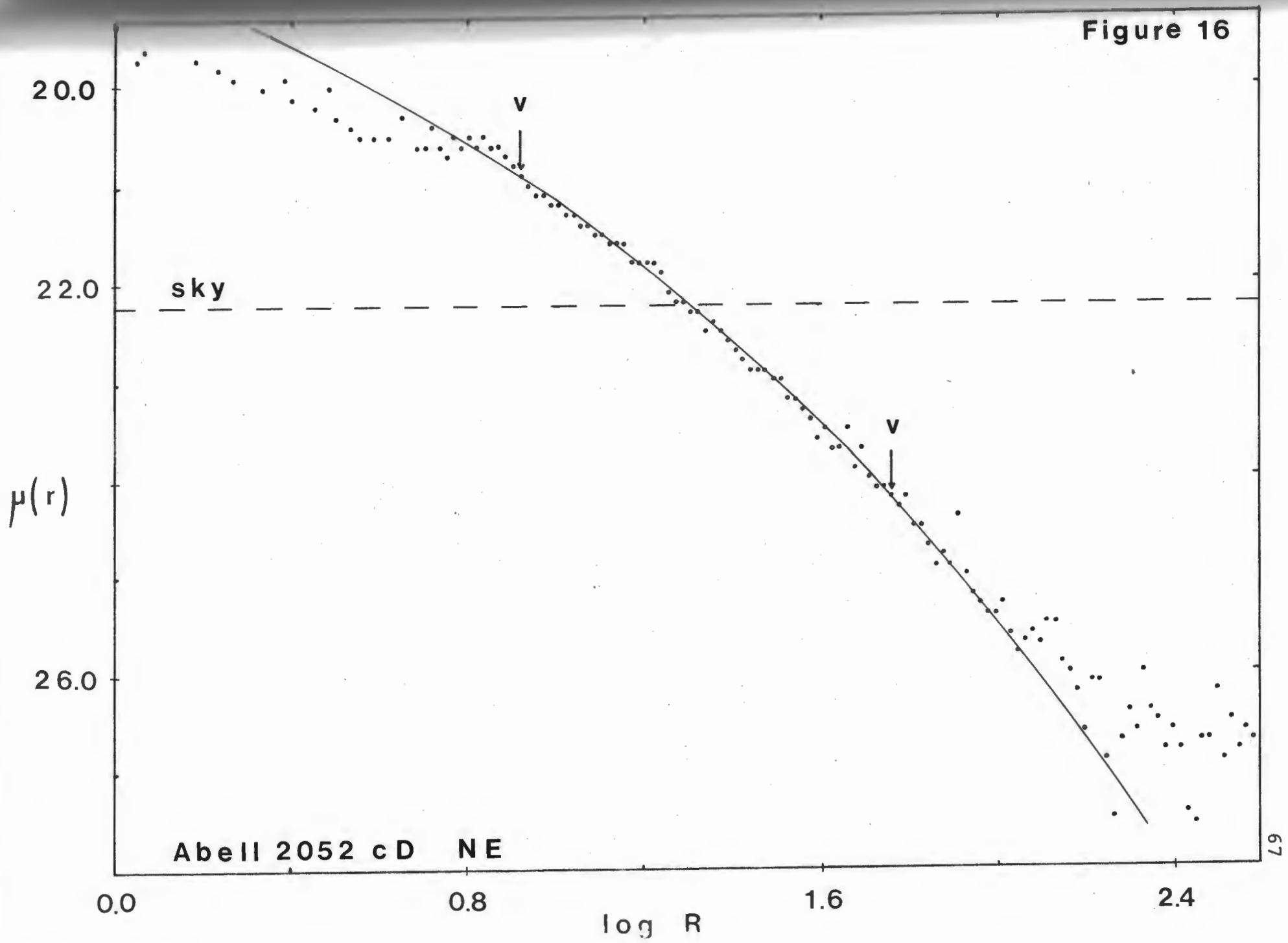
Figure 16
20.0
22.0
26.0
sky
v
v
μ(r)
Abell 2052 cD NE
0.0
0.8
1.6
2.4
log R
67

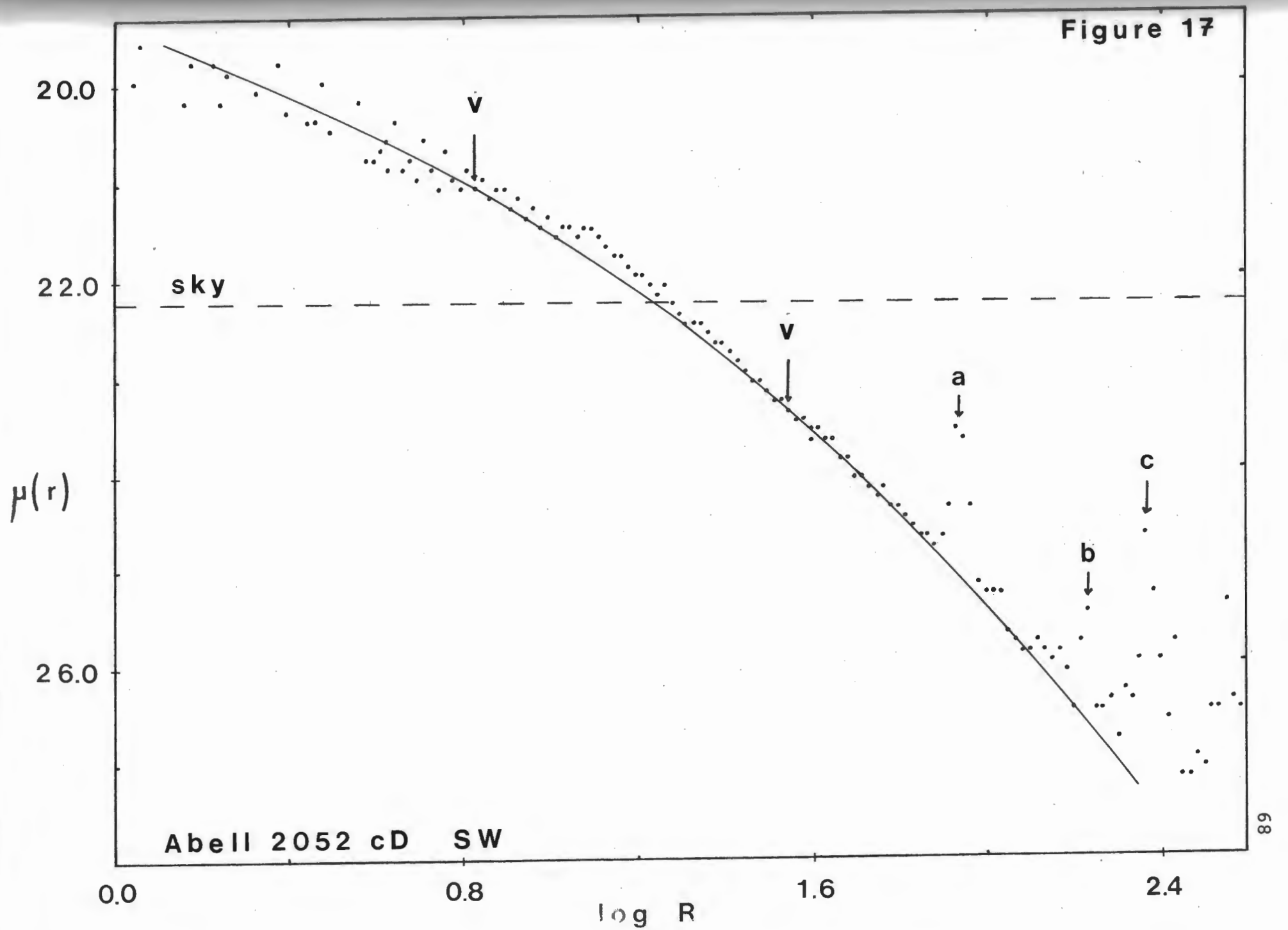
Figure 17
20.0
22.0
26.0
μ(r)
sky
v
v
a
b
c
Abell 2052 cD SW
0.0
0.8
1.6
2.4
log R
89

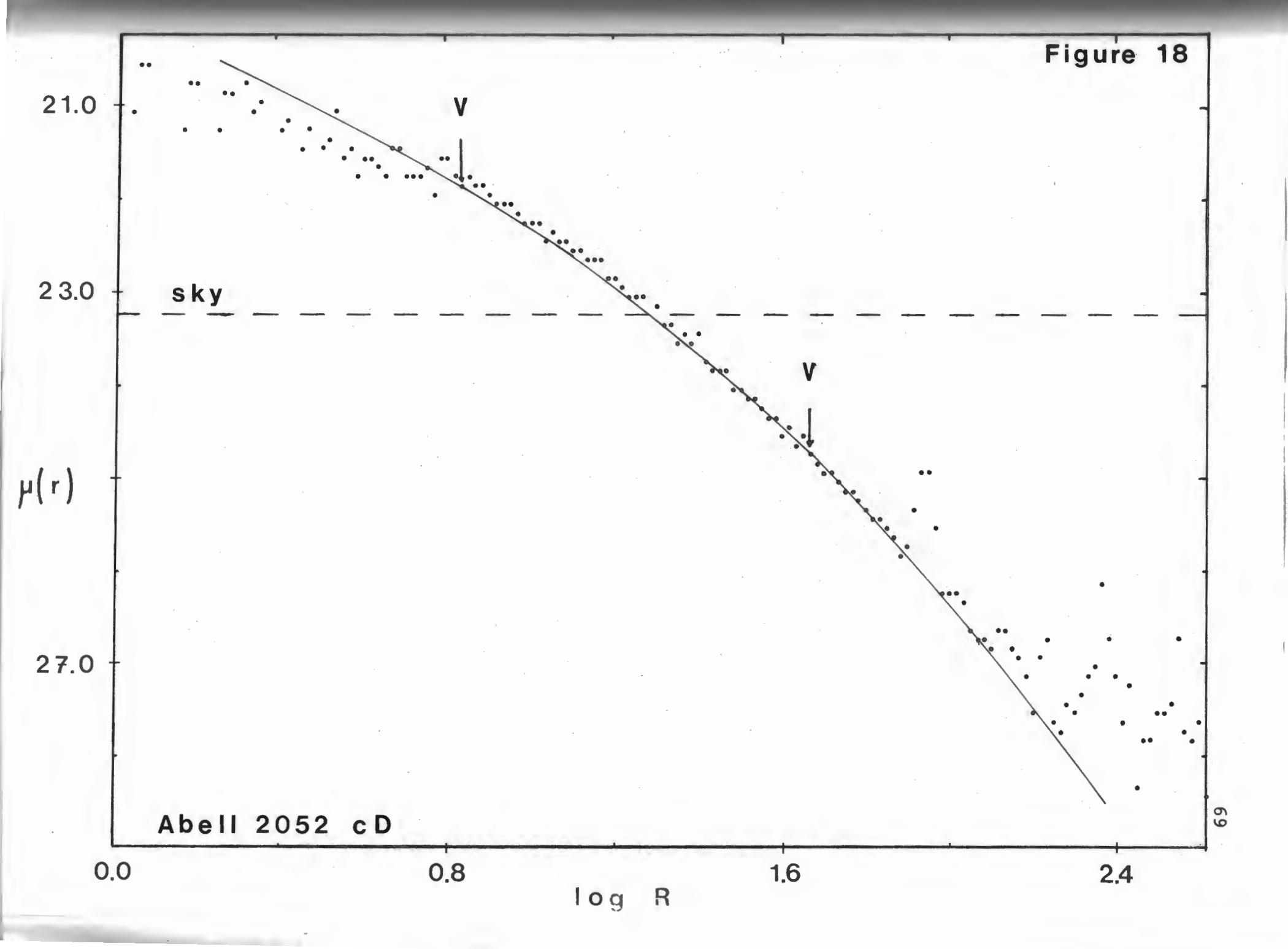
Figure 18
21.0
23.0
27.0
sky
V
V
μ(r)
Abell 2052 cD
0.0
0.8
1.6
2.4
log R
69

FIGURE 19: Surface brightness profile of the NE axis of the cD galaxy NGC 6166.

FIGURE 20: Surface brightness profile of the SW axis of the cD galaxy NGC 6166. "a" indicates the position of another galaxy superimposed on the axis profile.

FIGURE 21: Folded axes surface brightness profile of the two semi-axes of NGC 6166. "a" is the position of the light from another galaxy superimposed on the SW axis.

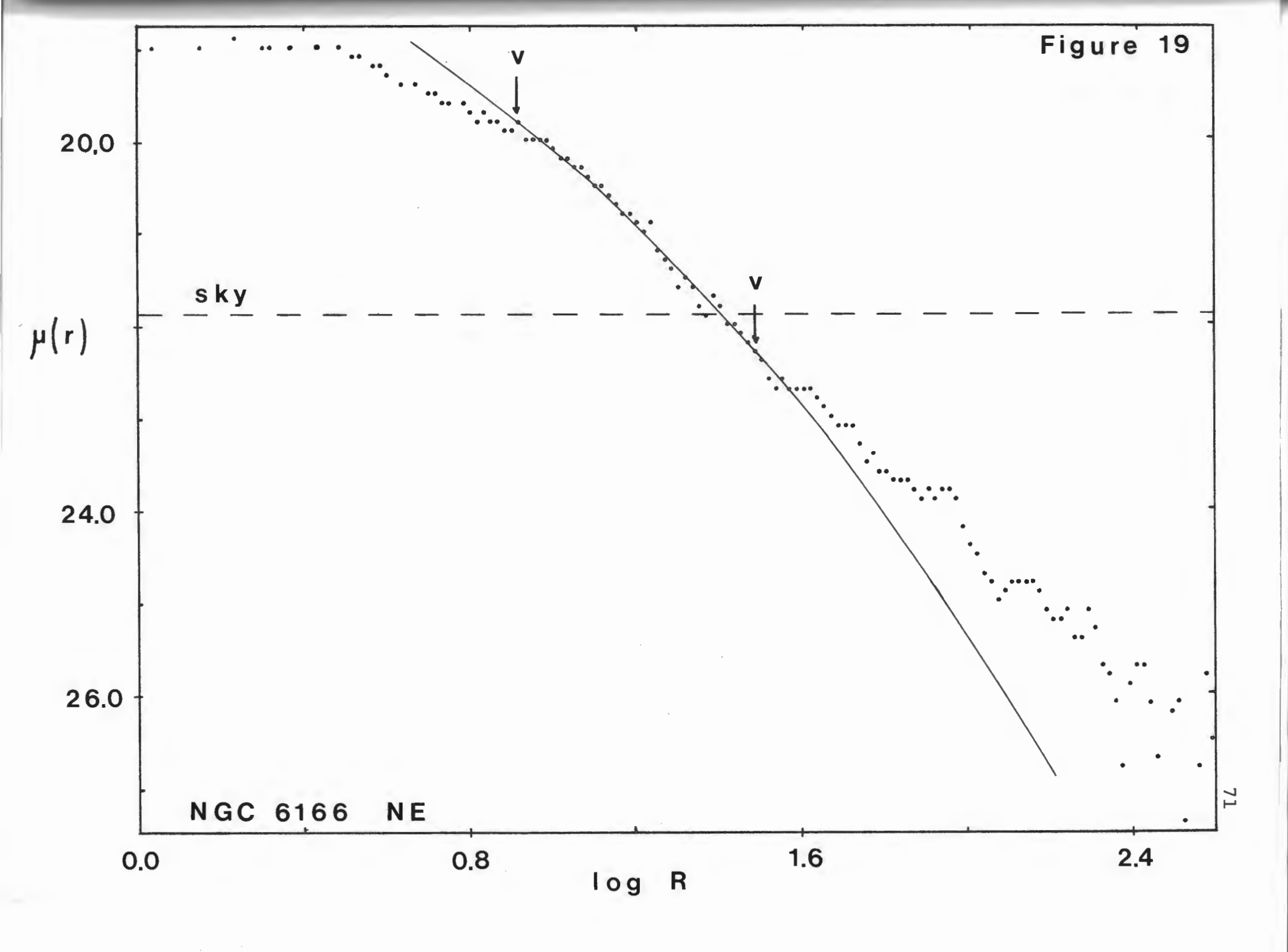
Figure 19
20.0
24.0
26.0
μ(r)
sky
v
v
NGC 6166 NE
0.0
0.8
1.6
2.4
log R
71

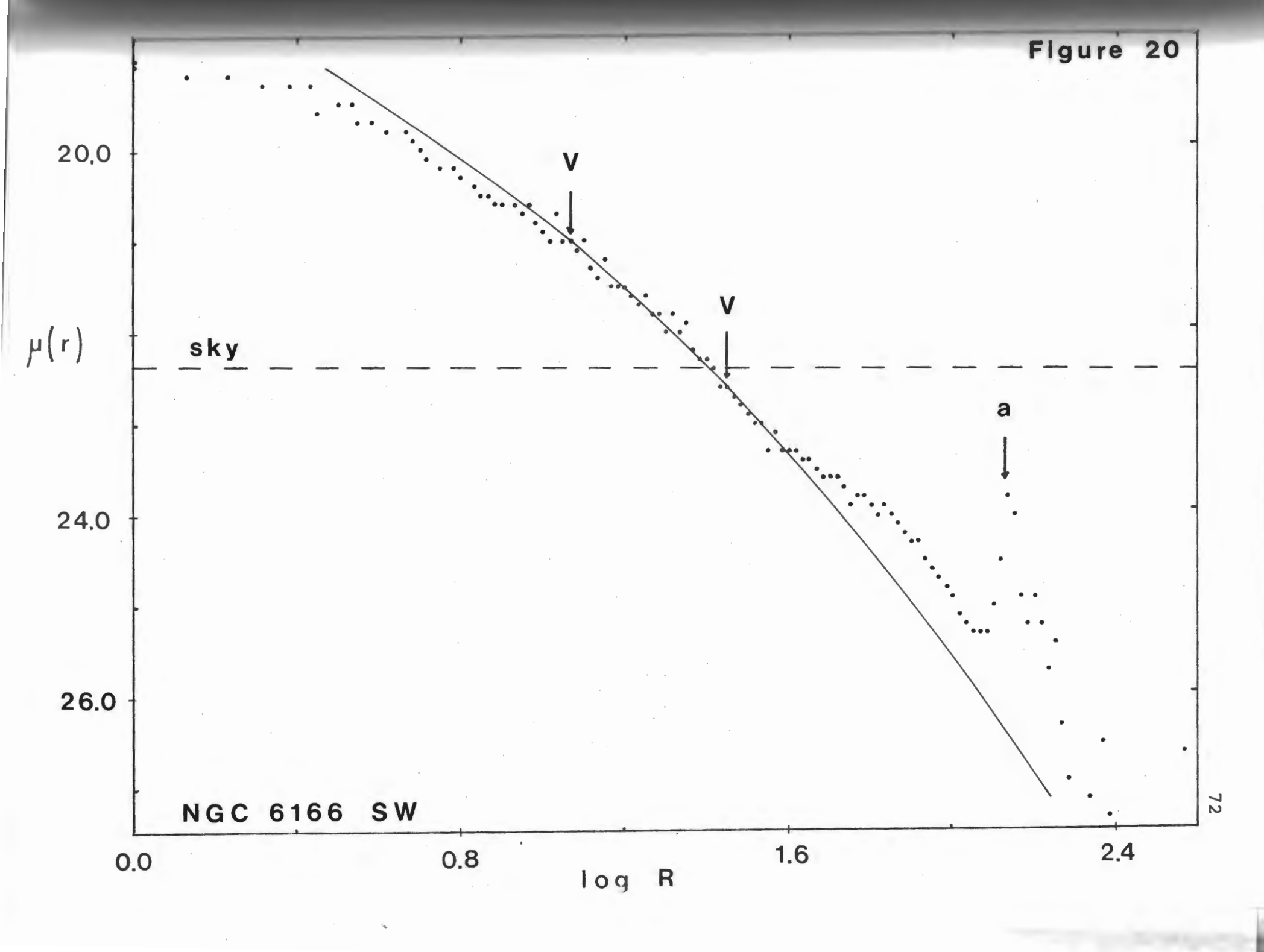
Figure 20
20.0
24.0
26.0
μ(r)
sky
V
V
a
NGC 6166 SW
0.0
0.8
1.6
2.4
log R
72

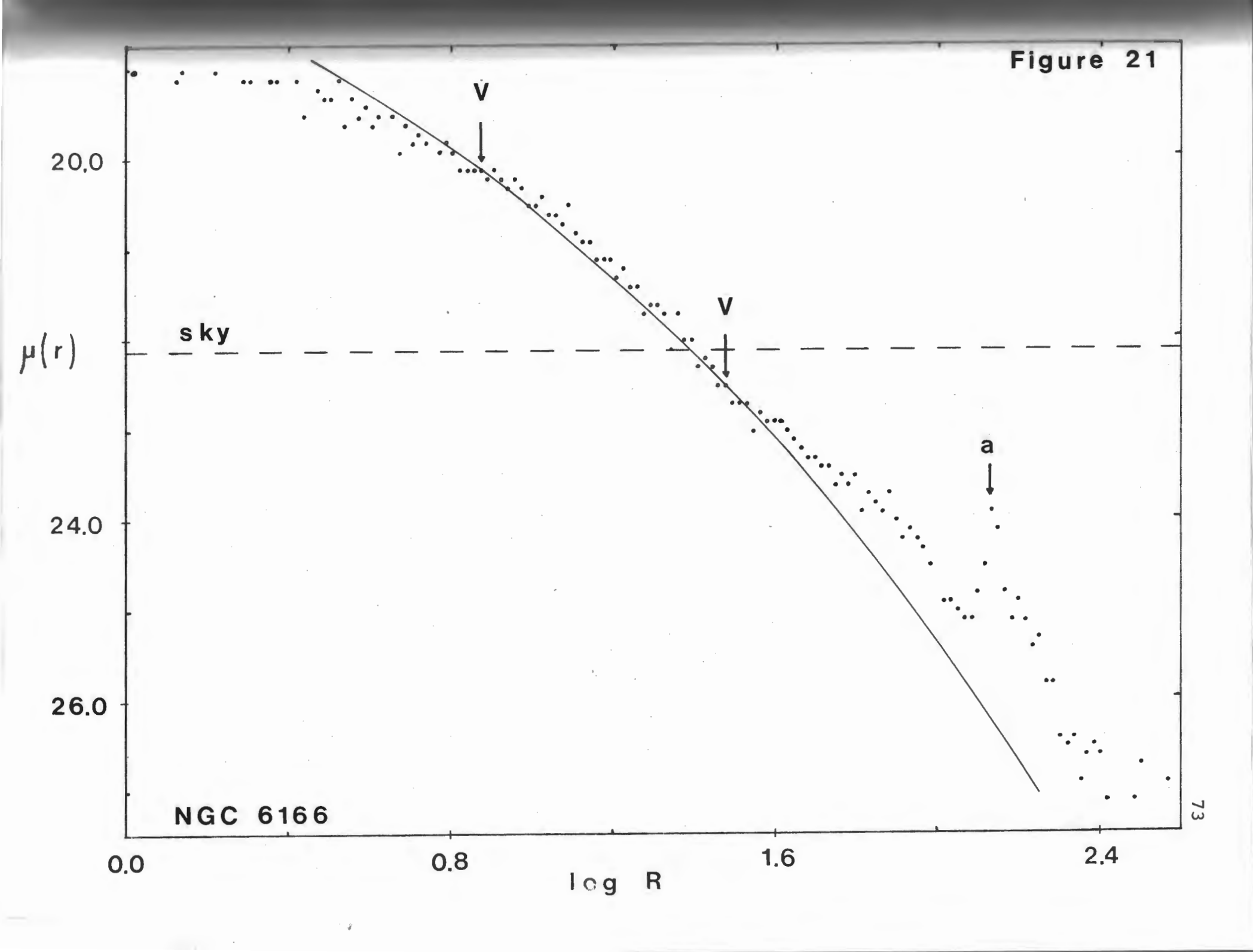
Figure 21
V
V
a
sky
μ(r)
20.0
24.0
26.0
NGC 6166
0.0
0.8
1.6
2.4
log R

seen from the folded profile in Figure 21, it displays the characteristic traits of fitting de Vaucouleurs' law at intermediate distances, while becoming progressively brighter than predicted at larger distances. The slope of the light distribution beyond log R $\sim$ 1.5 is -4.0, exactly as predicted by Bahcall. The flattened top portion of the profile within log R = 0.5 show a relatively low central surface brightness, typical of giant galaxies.

5.4 Conclusions

The results of the fitting procedures to de Vaucouleurs' law with the program elliptical galaxies have shown that there are no major reduction errors in this study. All but one of the elliptical galaxies fit the expected curves very well. The exception, identified as A-29/52 AC, was found to have an extended envelope not unlike those of giant elliptical and supergiant galaxies. The possession by a field galaxy of a halo whose light distribution resembles that of a cD galaxy and can be described by the Bahcall relation intended for supergiant galaxies, is a factor which must be considered in any theory of cD galaxy formation.

Of the four supergiant galaxies studied, only one (the cD galaxy in Abell 401) could not be described by the relation suggested by Bahcall. All program cD galaxies did, however, show exponential light distributions, therefore it may be

that the required relation to fit supergiant galaxy profiles should contain more than one fitting parameter.

If, however, the cD galaxy brightness profiles cannot all be described by the same empirical relation, the galaxies cannot have experienced the same dynamical history. They may still have had similar origins, but some have taken different evolutionary paths thereafter. These different paths would be dependent on the environmental conditions (eg. central galaxy density, and distribution of orbital eccentricities) in the vicinity of the cD galaxy.

There is another possibility. Since the surface brightness profile is a record of the distribution of stars in a galaxy, variations in the shapes of cD galaxy profiles may indicate differences in this distribution. This may be caused by the recent accretion of a smaller galaxy through dynamical friction, resulting in a transfer of the orbital kinetic energy of the victim to the halo of the cD galaxy. Such accretions would significantly perturb the halo, requiring several orbital periods ($\sim 10^9$ years) to damp out. It is possible that the cD galaxy in Abell 401 is experiencing such a phase. The damping process must be quite advanced, however, since the light distribution in the halo seems smooth and there is no evidence that the core of the victim is still intact.

Clearly, the question of the origin and formation of

supergiant galaxies is not an easy one to answer; much more work is needed. The existence in poor clusters, of galaxies whose brightness profiles resembles those of cD galaxies (eg. NGC 4073 in the cluster MKW-4), located on the shoulder of the cluster potential well (eg. NGC 4839 in the Coma cluster), and in the field (eg. A-29/52 AC), present a fundamental difficulty for all current theories of their origin.

REFERENCES

Abell, G.O. (1958) Ap.J. Suppl. 3, 211

Albert, C.E., White, R.A. and Morgan, W.W. (1977) Ap.J. 211, 309

Bahcall, N.A. (1977) Ann. Rev. Astr. Ap. 15, 505

Bautz, L.P. and Morgan, W.W. (1970) Ap.J. Lett. 162, L149

Carter, D. (1977) M.N.R.A.S. 178, 137

de Vaucouleurs, G. (1953) M.N.R.A.S. 113, 134

_____ (1974) in IAU Symp. No. 58, "The Formation and Dynamics of Galaxies", ed. J.R. Shakeshaft; Dordrecht: Reidel. p. 1

de Vaucouleurs, G. and de Vaucouleurs, A. (1964) Reference Catalogue of Bright Galaxies. Austin: University of Texas Press

Faber, S.M., Burstein, D. and Dressler, A. (1977) A.J. 82, 941

Gallagher, J. and Ostriker, J.P. (1972) Ap.J. 177, 288

Geller, M. (1974) Unpublished Ph.D. thesis, Princeton University

Gunn, J.E. and Oke, J.B. (1975) Ap.J. 195, 255

Hausman, M.A. and Ostriker, J.P. (1978) Ap.J. 224, 320

Jenner, D.C. (1974) Ap.J. 191, 55

King, I.R. (1962) A.J. 67, 471

Leir, A.A. and van den Bergh, S. (1977) Ap.J. Suppl. 34, 381

Nilson, P. (1973) Uppsala General Catalogue of Galaxies. Uppsala: Acta Universitatis Upsaliensis

Matthews, T.A., Morgan, W.W. and Schmidt, M. (1964) Ap.J. 140, 35

Minkowski, R. (1961) A.J. 66, 558

Morgan, W.W. (1958) Pub. A.S.P. 70, 364

Morgan, W.W., Kayser, S. and White, R.A. (1975) Ap.J. 199, 545

Morgan, W.W. and Lesh, J.R. (1965) Ap.J. 142, 1364

Oemler, A. (1973) Ap.J. 180, 11

_____ (1974) Ap.J. 194, 1

_____ (1976) Ap.J. 209, 693

Ostriker, J.P. and Hausman, M.A. (1977) Ap.J. Lett. 217, L125

Ostriker, J.P. and Tremaine, S.D. (1975) Ap.J. Lett. 202, L113

Page, T.L. (1961) Proc. Fourth Berkeley Math. Stat. and Prob. 3, 277

Peterson, B.A. (1970) A.J. 75, 695

Richstone, D.O. (1976) Ap.J. 204, 642

Sandage, A. (1961) Ap.J. 133, 355

_____ (1972) Ap.J. 178, 1

_____ (1976) Ap.J. 205, 6

Sandage, A. and Hardy, E. (1973) Ap.J. 183, 743

Strom, S.E. and Strom, K.M. (1976) Ap.J. 204, 684

Strom, K.M. and Strom, S.E. (1978a) A.J. 83, 73

Strom, S.E. and Strom, K.M. (1978b) A.J. 83, 732

Strom, K.M. and Strom, S.E. (1978d) A.J. 83, 1293

Zwicky, F., Herzog, E., Wild, P., Karpowicz, M. and Kwal, C.T. (1961-68) Catalogue of Galaxies and Clusters

of Galaxies. 6 volumes. Pascedena: California Inst. Tech.

APPENDIX A

Plate Material

PLATE #	EMULSION	FILTER	EXPOSURE	OBJECT FIELD
PS 5723	103a-D	Wr. 12	20 min.	NGC 4881
5736	103a-D	Wr. 12	20	Abell 2029/2052
5737	103a-D	Wr. 12	5	"
5738	103a-D	Wr. 12	20	Abell 2197/2199
5739	103a-D	Wr. 12	5	"
5741	103a-E	OR-1	60	NGC 4881
5747	103a-D	Wr. 12	5	"
5754	103a-E	OR-1	60	Abell 2029/2052
5755	103a-D	Wr. 12	20	Abell 2197/2199
5756	103a-D	Wr. 12	5	"
6861	IIIa-J	Wr. 4	990	NGC 4881
6863	IIIa-J	Wr. 2c	82	Abell 2197/2199
6868	IIIa-J	Wr. 4	120	Abell 2029/2052
6871	IIIa-J	Wr. 4	120	"
7135	103a-D	Wr. 12	20	Abell 401
7144	IIIa-J	Wr. 4	120	"
7167	103a-D	Wr. 12	5	"
7168	103a-D	Wr. 12	20	"
7169	IIIa-J	Wr. 4	120	"

APPENDIX B

Using PROFIL to Process Density Tracings

The data deck for PROFIL consists of two main parts. The first part contains the two control cards which govern the choice of averaging options for the computer run. The second is composed of the number NPLATE of tracing data files- one file for each density tracing to be processed.

(1) Data Control Cards

VARIABLE NAME	FORMAT	# CARDS	COMMENTS
NPLATE	I2	1	number of tracings to be processed
COMBIN	A10	1	NO AVERAGE - each axis plotted separately AVERAGE1ST - stacks first semi-axes AVERAGE2ND - stacks second semi-axes AVERAGEALL - averages the two semi-axes, then stacks with previous tracings

(2) Input Data Cards for Density Tracing File

The following is a list of all data file input required by the program PROFIL, giving the name of the variable, format of input, order of its appearance in the data file, and any necessary instructions or comments.

VARIABLE NAME	FORMAT	# CARDS	COMMENTS
tracing ID		1	
OBJT	A4	1	STAR or GLXY
NPRINT	I2	1	00 - full printout and plots 01 - minimum printout, plots >01 - data to be plotted and plots
NPTS, DINIT	I3,F8.1	1	NPTS - # points in characteristic curve DINIT- initial density (mm) of characteristic curve. points spaced 10mm in density
CURVE	10F8.2	3	relative intensity points from curve
SKYCAL	F5.1	1	sky density in mm above clear plate
ISKY	20I4	<28	sky density tracing points
IGAL	2I4	1	location of galaxy nucleus on sky tracing

VARIABLE NAME	FORMAT	# CARDS	COMMENTS
IOBJ	20I4	<28	galaxy (or star) density tracing
ICENTR	2I4	1	location of galaxy nucleus on galaxy tracing
NPLOT	I2	1	00 - no plots 01 - plots on some plotting device >01 - plots on line printer
DEL	F4.1	1	used only if NPLOT = 00 Minimum Values for DEL

Ratio Arm	DEL
200	00.2
100	00.4
50	00.7
20	02.0
10	04.0

APPENDIX C

Density Tracings to Produce Profiles

The following are lists of the density tracings used to produce the surface brightness profiles given in Figures 1 through 21.

"Ratio Arm" is the magnification of the tracing from the plate. "Slit Width" is the dimensions (in microns) of the projected microdensitometer slit. "Special Instructions" show the values required for the boundary criteria of the matching regions, and any changes to be made in the sky brightness level (TSKY).

OBJECT/ FILE NAME	PLATE #	RATIO ARM	SLIT WIDTH	SPECIAL INSTRUCTIONS AVERAGE1ST	AVERAGE2ND	AVERAGEALL
NGC 4881				5σ, 2slits	5σ, 2 slits	5σ, 2 slits
N488102	PS 5741	197.10	35x35μ			
N488104	5747	197.10	35x35			
N488106	5723	96.38	70x70			
N488108	6861	49.46	70x70			
Abell 401 cD				12.5σ, 1 slit	12.5σ, 1 slit	12.5σ, 1 slit
A40111	PS 7167	197.10	35x35μ			
A40112	7135	49.46	70x60			
A40113	7168	49.46	70x60			
A40115	7144	20.29	120x110			
A40117	7169	20.29	120x110			

OBJECT/ FILE NAME	PLATE #	RATIO ARM	SLIT WIDTH	SPECIAL INSTRUCTIONS AVERAGE1ST	AVERAGE2ND	AVERAGEALL
A-401 #1				12.5σ, 1 slit	12.5σ, 1 slit	12.5σ, 1 slit
A40132	PS 7135	96.38	70x60μ			
A40133	7168	96.38	70x60			
A40134	7144	49.46	70x60			
A40135	7169	49.46	70x60			
A-401 #2				12.5σ, 1 slit	12.5σ, 1 slit	12.5σ, 1 slit
A40142	PS 7135	96.38	70x60μ			
A40143	7168	96.38	70x60			
A40144	7144	49.46	70x60			
A40145	7169	49.46	70x60			

OBJECT/ FILE NAME	PLATE #	RATIO ARM	SLIT WIDTH	SPECIAL INSTRUCTIONS AVERAGE1ST	AVERAGE2ND	AVERAGEALL
A-401 #2				12.5σ, 1 slit	12.5σ, 1 slit	12.5σ, 1 slit
A40152	PS 7135	96.38	70x60μ			
A40153	7168	96.38	70x60			
A40154	7144	49.46	70x60	TSKY= 17.1	TSKY= 17.6	
A40155	7169	49.46	70x60	TSKY= 16.5	TSKY= 15.7	
Abell 2029 cD				12.5σ, 1 slit	12.5σ, 1 slit	12.5σ, 1 slit
A295212	PS 5737	197.40	25x35μ			
A295214	5736	49.46	70x70			
A295215	6868	20.29	120x120	TSKY= 14.3	TSKY= 17.0	
A295217	6871	20.29	120x120			

OBJECT/ FILE NAME	PLATE #	RATIO ARM	SLIT WIDTH	SPECIAL INSTRUCTIONS AVERAGE1ST	AVERAGE2ND	AVERAGEALL
Abell 2052 cD				20σ, 2 slits	20σ, 2 slits	20σ, 2 slits
A295221	PS 5754	197.40	35x35μ			
A295222	5737	197.40	25x35			
A295224	5736	49.46	70x70			
A295225	6868	20.29	120x120			
A295226	6871	20.29	120x120			
A-2952 #5				12.5σ, 1 slit	12.5σ, 1 slit	12.5σ, 1 slit
A295231	PS 5754	197.40	35x35μ			
A295232	5737	197.40	25x35			
A295233	5736	96.38	70x70			
A295234	6868	49.46	60x70	TSKY= 22.5		

OBJECT/ FILE NAME	PLATE #	RATIO ARM	SLIT WIDTH	SPECIAL INSTRUCTIONS AVERAGE1ST	AVERAGE2ND	AVERAGEALL
A-2952 AC				20σ, 2 slits	20σ, 2 slits	20σ, 2 slits
A295241	PS 5754	197.40	25x35μ			
A295242	5737	197.40	25x35			
A295243	5736	96.38	60x70			
A295244	6868	49.46	60x70	TSKY= 13.3	TSKY= 14.5	
NGC 6166				20σ, 2 slits	20σ, 2 slits	20σ, 2 slits
A219901	PS 5739	197.40	35x35μ			
A219902	5756	197.40	35x35			
A219903	5738	49.46	70x70			
A219904	6863	20.29	140x140			
A219907	5755	49.46	70x70			

OBJECT/ FILE NAME	PLATE #	RATIO ARM	SLIT WIDTH	SPECIAL INSTRUCTIONS AVERAGE1ST	AVERAGE2ND	AVERAGEALL
NGC 6146				20σ, 2 slits	20σ, 2 slits	20σ, 2 slits
A219932	PS 5739	197.40	35x25μ			
A219933	5756	197.40	35x35			
A219934	5738	49.46	70x70			
A219935	5755	49.46	70x70			
A219936	6863	20.29	120x120			
NGC 6160				20σ, 2 slits	20σ, 2 slits	20σ, 2 slits
A219942	PS 5739	197.40	35x25μ			
A219943	5756	197.40	35x35			
A219944	5738	49.46	70x70			
A219945	5755	49.46	70x70			
A219946	6863	20.29	120x120			

OBJECT/ FILE NAME	PLATE #	RATIO ARM	SLIT WIDTH	SPECIAL INSTRUCTIONS AVERAGE1ST	AVERAGE2ND	AVERAGEALL
NGC 6173				20σ, 2 slits	20σ, 2 slits	20σ, 2 slits
A219952	PS 5739	197.40	35x25μ			
A219953	5756	197.40	35x35			
A219954	5738	49.46	70x70			
A219955	5755	49.46	70x70			
A219956	6863	20.29	120x120			

APPENDIX D

Running PROFIL

The program RUNDAL contains all the necessary commands to run the program PROFIL in batch mode on the Dalhousie University CDC 6400 computer.

The density tracing files are arranged in the order they are to be stacked after the options NPLATE and COMBIN, and these are all stored in a single data file DATA1. When submitted to batch, RUNDAL calls the file BRT1, which contains PROFIL, then calls DATA1. The program is then excecuted and a printout of the run made on the Dalhousie Computer Centre's lineprinter.

```
 79/07/15. 16.30.22.
PROGRAM  _ RUNDAL

/JOB
APROFIL,T070,CM11000.    G.WELCH
ACCOUNT,SMAS004,GALAXY.
GET(BRT1)
GET(DATA1)
FTN(I = BRT1, PL = 7000, OPT = 1, L = 0)
RFL(110000)
LGO(DATA1)
EXIT.
/EOF
READY.
```

APPENDIX E

Sample PROFIL Stacking Run

The following is an example of a typical stacking run with PROFIL. It is the folded axes option AVERAGEALL of four plates of the cD galaxy in Abell 2029.

Each page represents the stacking of one plate. The first plot of each page is a superposition of the profile of each semi-major axis. The second plot is the averaged profile of the two semi-axes, stacked with the cumulative average of the previous plates. For a more detailed description of the information included in the stacking run, refer to section 3.3.

APPENDIX F

The Program ITERATE

ITERATE was written to calculate the scaling factors used in the calibration of the surface brightness profiles. Input data is in the form of a data file, in the format shown below. An initial value for b is required to begin the iterations. After each iteration, b is printed out so that convergence to the correct value can be seen.

VARIABLE NAME	FORMAT	COMMENTS
NGAL	I4	galaxy identification
B	F6.3	initial value for scaling factor
NPHOT	I2	number of isophotes used
PHMAG	F5.2	photometric magnitude
INUM	I2	number of iterations
APDIAM	F5.1	photometric aperture diameter
IAXIS	A2	axis identification
AREA	F6.2	isophotal area (in square arcseconds)
AVMAG	F8.3	average magnitude of isophote

```
 79/07/15. 16.17.07.
PROGRAM   ITERATE

00100 PROGRAM ITERATE(INPUT,OUTPUT,THX66A,TAPE1=THX66A)
00102C      THIS PROGRAM IS USED TO CALCULATE THE SCALING FACTORS
00103C  OF THOSE GALAXIES FOR WHICH PHOTOELECTRIC PHOTOMETRY
00104C  AND ISODENTS ARE AVAILABLE.  THE SCALING FACTOR B IS
00105C  THAT NUMBER IN MAGNITUDES WHICH IS ADDED TO THE RELATIVE
00106C  INTENSITY SCALE TO OBTAIN ABSOLUTE INTENSITY CALIBRATION.
00107C
00110 DIMENSION AREA(50), AVMAG(50)
00120 READ(1,100) NGAL,B,NPHOT,PHMAG,INUM,APDIAM,IAXIS
00130 PRINT 200, NGAL, PHMAG
00140 PRINT 201, APDIAM
00150 PRINT 202, IAXIS, NPHOT
00160 PRINT 205, INUM, B
00170 DO 30 I=1, NPHOT
00180 READ(1,110) AREA(I), AVMAG(I)
00190 30 CONTINUE
00200 E = 2.71828183
00210 DO 20 K=1,INUM
00220 SUM1 = 0.0
00230 SUM2 = 0.0
00240 DO 10 J=1,NPHOT
00250 SUM1 = SUM1 + (AREA(J)*10**((AVMAG(J)+B)/(-2.5)))
00260 SUM2 = SUM2 + AREA(J)
00270 10 CONTINUE
00280 ZNUM = 2.5*ALOG10(SUM1) + PHMAG
00290 ZDEMO = ALOG10(E)*ALOG(10*SUM2)
00300 B = B + (ZNUM/ZDEMO)
00310 PRINT 210, K, B
00320 20 CONTINUE
00330 100 FORMAT(I4,2X,F6.3,2X,I2,2X,F5.2,2X,I2,2X,F5.1,2X,A2)
00340 110 FORMAT(F6.2,2X,F8.3)
00350 200 FORMAT(3HNGC,I4,6X,9HMAGNITUDE,2X,F5.2)
00360 201 FORMAT(18HAPERATURE DIAMETER,2X,F5.1,7H ARCSEC)
00370 202 FORMAT(A2,6H AXIS ,9HCONTAINS ,I2,10H ISOPHOTES)
00380 205 FORMAT(I2,1X,25HITERATIONS BEGIN WITH B = ,F8.3)
00390 210 FORMAT(5X,I2,F15.8)
00400 STOP
00410 END
READY.
```

APPENDIX G

The Program ICENTR

Since the production of the density tracings and their digitization was not done with the same machine, or with the tracing paper in the same position, frequently there was a difference in the angle as well as the position of the origin of the tracing and digitization coordinate systems. The coordinates of ICENTR (the position of the centre of the galaxy) as printed in the data deck (originally chosen by eye during the digitizing) had to be rotated and translated to the tracing coordinate system before they could be used for calibration purposes.

The program ICENTR was written to accept the grid points of the tracing in the system of the digitizer, then calculate the angular difference between the systems. Several pairs of points of equal density are input, and the program averages each pair of numbers and translates the averages to the tracing coordinate system. The X coordinates are then averaged to produce the new ICENTR position in the tracing system. The list below show the required data and the formats which are to be used for their input.

VARIABLE NAME	FORMAT	COMMENTS
IGD	6I4	tracing grid points (6)
NCPT	I2	number of pairs of points to be used
XC1, YC1	2F5.0	X and Y coordinates of first point of pair
XC2, YC2	2F5.0	X and Y coordinates of second point of pair

```
 79/07/18. 16.26.34.
PROGRAM   ICENTR

00100     PROGRAM ICENTR(INPUT,OUTPUT,QUIRK,TAPE1=QUIRK)
00110C      THE FOLLOWING PROGRAM IS USED IN CALIBRATING AN UNKNOWN
00120C  FROM A KNOWN GALAXY.  IT CALCULATES THE ANGLE OF ROTATION
00130C  OF THE GALAXY TRACING W.R.T. THE DIGITIZER, AND PRODUCES
00140C  THE NEW VALUE OF THE NUCLEUS POSITION (ICENTR) FROM THE
00150C  TRACING GRID COORDINATES AND THE UNROTATED VALUE OF ICENTR.
00160C
00170 DIMENSION IGD(6),GD(6),XC1(10),YC1(10)
00180 DIMENSION XC2(10),YC2(10),RC(10),YC(10),XCP(10),XC(10)
00190C  FIND ANGLE OF ROTATION
00200 READ(1,100) (IGD(I),I=1,6)
00210 Y1 = IGD(6) - IGD(4)
00220 X1 = IGD(5) - IGD(3)
00230 THETA1 = ATAN(Y1/X1)
00240 X2 = IGD(2) - IGD(4)
00250 Y2 = IGD(3) - IGD(1)
00260 THETA2 = ATAN(Y2/X2)
00270 THETA = (THETA1 + THETA2))/2.0
00280C  FIND ICENTR IN TRACING COORD. SYSTEM
00290 READ(1,110) NCPT
00300 CENTR = 0.0
00310 DO 20 J = 1, NCPT
00320 READ(1,120) XC1(J), YC1(J), XC2(J), YC2(J)
00330 XC = (XC1(J) + XC2(J))/2.0
00340 YC = (YC1(J) + YC2(J))/2.0
00350 RC(J) = SQRT(XC(J)**2 + YC(J)**2
00360 ALPHA = ACOS(XC(J)/RC(J))
00370 XCP(J) = RC(J)*COS(ALPHA - THETA)
00380 CENTR = CENTR + XCP(J)
00390 20 CONTINUE
00400 ZNCPT = NCPT
00410 CENTR = CENTR/ZNCPT
00420 GD(3) = IGD(3)
00430 CENTR = (CENTR - GD(3))/10.0
00440 ANGLE = THETA * 57.3
00450 PRINT 200, ANGLE
00460 PRINT 210, CENTR
00470 100 FORMAT(6I4)
00480 110 FORMAT(I2)
00490 120 FORMAT(4F5.0)
00500 200 FORMAT(5X,28HANGLE BETWEEN COORD. SYSTEMS, F6.1//)
00510 210 FORMAT(5X,9HICENTR IS, F6.1, 25HMM. IN THE TRACING SYSTEM)
00520 STOP
00530 END
READY.
```